A New Combined Detection Algorithm for Blocking and Subtropical Ridges

PEDRO M. SOUSA,[a,b] DAVID BARRIOPEDRO,[c] RICARDO GARCÍA-HERRERA,[c,d] TIM WOOLLINGS,[e] RICARDO M. TRIGO[a,f]

[a] *Instituto Dom Luiz, Faculdade de Ciências, Universidade de Lisboa, Portugal*
[b] *Instituto Português do Mar e da Atmosfera (IPMA), Lisboa, Portugal*
[c] *Instituto de Geociencias, IGEO (CSIC-UCM), Madrid, Spain*
[d] *Departamento de Física de la Tierra y Astrofísica, Facultad de Ciencias Físicas, Universidad Complutense de Madrid (UCM), Madrid, Spain*
[e] *Department of Physics, Atmospheric, Oceanic and Planetary Physics, University of Oxford, Oxford, United Kingdom*
[f] *Departamento de Meteorologia, Instituto de Geociências, Universidade Federal do Rio de Janeiro, Rio de Janeiro, Brazil*

(Manuscript received 20 August 2020, in final form 17 May 2021)

ABSTRACT: Blocks are high-impact atmospheric systems of the mid-/high latitudes and have been widely addressed in meteorological and climatological studies. However, the diversity of blocking definitions makes comparison across studies not straightforward. Here, we propose a conceptual model for the life cycle of high pressure systems that recognizes the multifaceted and transient characteristics of these events. A detection scheme identifies and classifies daily structures, discriminating between subtropical ridges and different types of well-established blocking patterns (omega and dipole-like Rex). This is complemented by a spatiotemporal tracking algorithm, which accounts for transitions between patterns, providing a global catalog of events for 1950–2020. Criteria rely on simple metrics retrieved from one single-level field, and allow implementation in different datasets and climatic realms. Using reanalysis data, we provide illustrative examples, the first global and seasonal climatological assessment of the diversity of high pressure events, their associated impacts, and recent frequency changes. Results reveal that ridge and blocking events affect widespread regions from the subtropics to high latitudes. We find remarkably distinct regional impacts among the considered types, which had been hindered in previous studies by restricted focus on Rex-like structures. This plethora of high pressure systems is much less evident in the Southern Hemisphere, where activity is dominated by subtropical ridges and secluded blocking-like patterns. We report increasing frequencies of low-latitude systems, although with hemispheric and seasonal differences that can only be partially interpreted as a consequence of subtropical expansion. Blocking frequency trends exhibit more heterogeneous and complex spatial patterns, with no evidence of generalized significant changes.

KEYWORDS: Atmosphere; Blocking; Climate classification/regimes; Algorithms

1. Introduction

Blocking and the associated disruption of the usual westerly flow is among the most high-impact atmospheric regimes in middle and high latitudes, and represents key challenges in numerical weather prediction, subseasonal-to-seasonal predictions and regional projections of climate change (e.g., Woollings et al. 2018). There is consensus on the importance of blocking, and its driving role in a wide diversity of extreme events, including summer heatwaves, winter cold spells, poor air quality episodes, pervasive droughts, flooding, and devastating hurricanes. Blocking is also a focus in currently active areas of research, such as the remote effects of Arctic amplification, marine heatwaves, or atmospheric rivers [see references in, e.g., Woollings et al. (2018)]. This wide interest and the lack of a unified theory for blocking has led to a wide diversity of atmospheric patterns termed "blocking," which makes the comparison across studies not straightforward with potentially diverging results in terms of observed changes, associated impacts, or future projections (e.g., Christensen et al. 2013).

The disagreement on what should be considered a block has created confusion in the scientific community, which translates to the media during devastating "blocking-related" extremes, such as the European mega-heatwave of 2003 (e.g., García-Herrera et al. 2010; Liu et al. 2018). Although the near-surface impacts of high-latitude blocks are well documented, recent studies have questioned the attribution of some extreme episodes to "classical" blocking in southern Europe (Sousa et al. 2018) and other Mediterranean-like climate zones such as California (Teng and Branstator 2017; Swain et al. 2016; Seager et al. 2015), Chile (Garreaud et al. 2019) or Australia (Timbal and Drosdowsky 2013; Marshall et al. 2014). In these midlatitude regions, temporary poleward intrusions of the subtropical belt (so-called subtropical ridges) become confounded with blocking. Despite the lack of definitive theoretical grounds to discriminate them, the distinction is useful from an impact-oriented perspective, since high-latitude blocks and subtropical ridges cause different and even opposite impacts in some regions and seasons (Sousa et al. 2017, 2018a). For example, while southern Europe experiences wet and cold conditions during canonical blocking, subtropical ridges almost completely wipe out precipitation and result in well

Supplemental information related to this paper is available at the Journals Online website: https://doi.org/10.1175/JCLI-D-20-0658.s1.

Corresponding author: Pedro M. Sousa, ppsousa@fc.ul.pt

DOI: 10.1175/JCLI-D-20-0658.1

above-average temperatures therein (Santos et al. 2009; Sousa et al. 2018a). The disentanglement of high pressure patterns becomes particularly important under the ongoing global warming, the ''tug-of-war'' effects of tropical/subtropical expansion and Arctic amplification in the midlatitudes, and the expected opposite responses of regional subtropical ridges and high-latitude blocks to increasing greenhouse gas concentrations (Li et al. 2012; Woollings et al. 2018). Despite this, subtropical ridges remain widely unexplored and there is a lack of comprehensive global studies devoted to these structures. Accounting for subtropical ridges in turn requires addressing transitions between these ''open ridges'' and blocking, as illustrated by the case studies discussed in Liu et al. (2018). This highlights the need for a more inclusive dynamical approach of high pressure systems, as we attempt here.

Many studies have proposed different definitions to detect classical high-latitude blocking in the midtroposphere (e.g., Dole and Gordon 1983; Tibaldi and Molteni 1990; Barriopedro et al. 2010; Barnes et al. 2012; Dunn-Siguoin et al. 2013). More recent works have incorporated potential vorticity frameworks and the concept of wave breaking, and have expanded the detection to the midlatitudes (e.g., Pelly and Hoskins 2003; Schwierz et al. 2004; Davini et al. 2012; Masato et al. 2012). The plethora of indices and systems referred to as blocking has motivated recurrent reviews (e.g., Barriopedro et al. 2010; Barnes et al. 2012; Woollings et al. 2018; Pinheiro et al. 2019), which agree on the diversity of patterns captured by different indices, but with limited advance toward a unified definition or agreement on the terminology. Instead, it seems we are advocated to acknowledge this diversity and recognize that different indices capture different aspects of this complex multifaceted phenomenon. A corollary is that different definitions must be used to make robust statements. One of the largest discrepancies concerns low-latitude structures with a flow reversal, typically referred to as ''low-latitude blocks'' (e.g., Davini et al. 2012; Pinheiro et al. 2019), which share some resemblance with subtropical ridges. However, it is clear that not all subtropical ridges exhibit a reversed zonal flow. In contrast to high-latitude blocking, the few attempts to identify subtropical ridges use tailored definitions for specific regions (Santos et al. 2009; Woollings et al. 2011; Sousa et al. 2018a) and lack the spatial structure of the event and its evolution. By relying on departure fields and regional anomaly thresholds, these definitions cannot be extrapolated to other regions, as well as models and periods with different climate realms.

Acknowledging the difficulty to make generalized statements about blocking due to the everlasting definition problem, herein we make a step forward and tackle current demands by the scientific community, as summarized by Woollings et al. (2018): ''Firstly, a blocking definition should be inclusive, identifying but differentiating between all types of blocks (i.e. with different structures, in different regions and seasons). In this sense, there remains the challenge of distinguishing among high-low dipoles, omega blocks and even open ridges. Secondly, the use of thresholds should be kept at a minimum and derived from the input data to accommodate seasonal and long-term variations and allow the applicability of the method to different climate states'' (p. 292). Revisiting the aforementioned literature and case studies it becomes clear that open ridges and classical blocking-like structures often appear during the evolution of the same anomalous high pressure event. Indeed, the former often precede wave-breaking events, whose mature expression is characteristic of blocking. Therefore, from a dynamical point of view, it is reasonable to consider subtropical ridges and blocks as related phenomena, while still discriminating them (e.g., Liu et al. 2018).

To the best of our knowledge, there are no studies that simultaneously address and distinguish blocking structures in a systematic way, and the transitions between these patterns. Here we present an inclusive conceptual model for the life cycle of high pressure events that accommodates the wide diversity of patterns recognized as blocks. An automated procedure is built upon this holistic multifaceted model, allowing the identification and discrimination of open ridges and flow-reversed blocking patterns, as well as different types of blocks. The method distinguishes the type of structure at daily scales and allows for transitions between the different types of structures during the life cycle of the high pressure event. Important assets of the method are its simplicity in terms of input data, and flexibility to be run for different periods and datasets, including past and future model simulations. Using reanalysis datasets, we provide illustrative examples, accessible catalogs, and the first global climatological assessment of the different types of structures, their associated impacts, and long-term frequency trends.

Section 2 describes the conceptual model for the life cycle of high pressure events in the middle troposphere, which sets the grounds for the methodological design of the detection scheme and the derived catalog of events. In section 3, the climatology and seasonal trends of each type of event are presented for each hemisphere. The associated near-surface impacts are discussed in section 4, where we also illustrate some case studies. Finally, section 5 summarizes the main results and discusses a range of future applications.

2. Data and methods

a. *Meteorological data*

Daily mean meteorological fields were retrieved from the NCEP–NCAR reanalysis dataset (Kalnay et al. 1996) on a 2.5° × 2.5° horizontal resolution grid for the 1950–2020 period. The following variables were considered: geopotential height at 500 and 1000 hPa (Z500 and Z1000, respectively), 2-m temperature (T2M), precipitation rate (PRE), and 300-hPa horizontal wind vector (UV300). These fields were used to characterize ridges and blocks (Z500) and to assess their near-surface impacts (T2M, PRE, Z1000) and jet stream configurations (UV300).

To assess the consistency of the results obtained with NCEP–NCAR, we also employed Z500 data from the ERA5 reanalysis (Copernicus Climate Change Service 2017) for the 1980–2020 period. This dataset was bilinearly interpolated

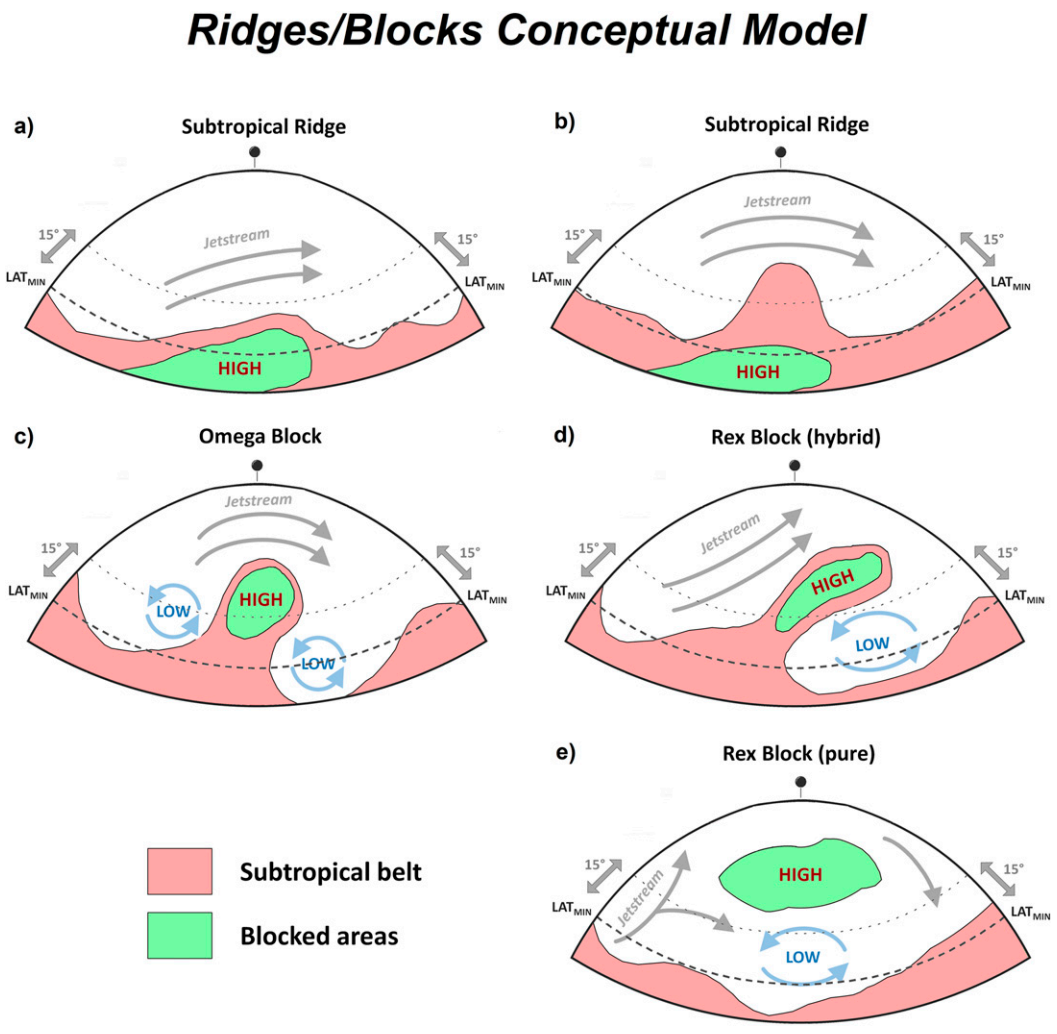

FIG. 1. Conceptual model of high pressure patterns describing a typical life cycle of an event in the NH, including the initial stages as a subtropical ridge, the development of flow reversals with omega shapes after a wave breaking, and mature phases as an isolated split-flow Rex block. Pink shading corresponds to air masses with subtropical characteristics, while green areas represent blocking of the extratropical westerlies by flow reversals in the middle troposphere. LAT_{MIN} represents the minimum latitude for detection (the zonal mean position of the subtropical belt edge). Gray and blue arrows denote typical synoptic features.

to the NCEP–NCAR grid before performing additional computations.

b. A conceptual model for ridge-blocking phenomenology

Subtropical ridges are herein considered temporary poleward extensions of the subtropical high pressure belt. These subtropical systems occasionally develop wave breaking, leading to the onset of a blocking event. Figure 1 illustrates a conceptual model for an idealized life cycle of such an event, including the early stages of a subtropical ridge, the development of an anticyclonic wave breaking, and a mature Rex block (fully isolated from the subtropical belt), as inferred from the inspection of single events and the revisited literature.

A subtropical ridge features an intrusion of the high pressure belt beyond its zonal mean latitude (LAT_{MIN}). Poleward extensions with no wave breaking or relatively shallow intrusions of the subtropical belt in the midlatitudes are thus considered a subtropical ridge, as depicted in Figs. 1a and 1b. These structures are generally associated with a strong jet stream on their poleward flank, resembling the low-latitude blocks described in previous works (e.g., Davini et al. 2012). They may or may not evolve into a block, depending on the subsequent development of wave breaking on synoptic scales.

The occurrence of wave breaking sets the onset of blocking (Figs. 1c–e). The early stage of a blocking can still display strong westerlies upstream of a high that is not fully secluded from the tropical belt, depicting the so-called omega shape appearance, with low pressure systems on its western and eastern flanks (Fig. 1c). At this stage, the system is not fully isolated from the subtropical belt and a relatively widespread

high pressure area is observed between the midlatitudes and the subtropics.

An omega block may or may not further evolve into a cutoff high, depending on the seclusion of the high pressure system. If this occurs, the structure becomes fully detached from the subtropics and exhibits pronounced meridional flow reversals to the south (Fig. 1e). At this stage, a widespread low pressure area develops between the blocking high and the subtropics, and a ''split flow'' of the jet stream is frequently observed upstream. This north–south dipole pattern can be classified as a ''canonical'' Rex block. A thorough inspection of these events revealed that the transition from an omega to a Rex block can temporarily exhibit ''mixed'' patterns, characterized by a tilted structure reminiscent of an omega block and large areas of flow reversal typical of ''pure'' Rex. These patterns are herein termed Rex-hybrid blocks (Fig. 1d). Rex-pure and Rex-hybrid blocks represent subtypes of the same structure (Rex blocks) and hence they will be considered together (and simply referred to as Rex blocks), unless otherwise stated.

Like any meteorological conceptual model, this one aims to illustrate the most relevant stages of an atmospheric process in an idealized way. Naturally, there might be events that do not follow this scheme, and some intricacies exist. For example, not all the structures go through all the stages of the model. Ridges do not necessarily evolve into a mature block (e.g., the western European June 2019 heatwave; Sousa et al. 2019), and omega blocks may not precede a mature Rex block (e.g., the persistent anticyclonic pattern fostering the 2004–05 Iberian drought; García-Herrera et al. 2007). Also, persistent high-latitude blocking-like patterns such as those associated with quasi-permanent seasonal features (e.g., the Siberian high or polar anticyclones; Takaya and Nakamura 2005; Wang et al. 2010; Cheung et al. 2013) may require little intervention of the subtropical belt. Moreover, the conceptual model of Fig. 1 does not preclude phase changes to occur within the different stages of the temporal sequence. For example, blocks can be re-absorbed by the subtropics, generating a new ridge, or connect to an existing one. Despite the multiple transitions and eventualities that can arise during the life cycle of an event, our exhaustive analyses and a review of the literature support that they can be well summarized by the three major categories shown in Fig. 1: subtropical ridges, omega blocks, and Rex blocks.

The algorithm is designed to identify and classify daily structures based on relatively simple metrics. Some of them are well established from extensive assessments and previous reviews of blocking indices. However, they present inherent limitations to capture the different stages of the conceptual model. As such, these metrics have been further developed herein to distinguish different types of blocks, and complemented with a novel approach that for the first time allows a global assessment of subtropical ridges. This holistic approach of subtropical and extratropical circulation provides an integral view of high-impact high pressure systems. The identified daily structures can be fully tracked regardless of their typology, therefore forming individual life cycles of high pressure events, each one characterized by its own spatiotemporal evolution and ''phase'' transitions, which provides a useful tool for the assessment of extreme events. Figure 2 provides a flowchart with the main steps and criteria involved in the process, from the local detection to the categorization of 2D structures.

c. Local ridge detection

Subtropical ridges are defined as poleward extensions of the subtropical belt into the middle and high latitudes. This in turn requires the delimitation of the subtropical belt. To explicitly detect areas embedded in the subtropical belt, we considered a straightforward approach based on the Z500 field. Herein, the subtropical belt is defined as areas where the instantaneous local Z500 value is higher than the hemisphere-wide mean Z500 averaged over the previous 15 days (see also Fig. 2):

$$Z500_{(\lambda,\phi,d)} > \overline{[Z500]}, \tag{1}$$

where λ, ϕ, and d represent longitude, latitude, and day, respectively. From now on, ϕ represents the modulus of latitude (i.e., in degrees relative to the equator), thus being applicable in the same way to both hemispheres. Square brackets denote the spatial (area-weighted) mean over the corresponding hemisphere (90°–0°N and 0°–90°S for the Northern and Southern Hemispheres, hereafter NH and SH, respectively), and the overbar denotes the time average for the $[d - 15, d - 1]$ interval, therefore excluding the diagnosed day from the definition. After testing different approaches and time averages, this 15-day period was considered because it is sufficiently long to filter transient features, and short enough to avoid biases in the seasonal cycle that would result from the use of backward averages over longer periods (see Fig. S1 in the online supplemental material). Despite being based on immediate states, $\overline{[Z500]}$ captures well the seasonal cycle of the climatological Z500 field (Fig. S1a), with the additional advantage that it does not require preprocessing and accommodates the Z500 rises induced by warming trends (Fig. S1b). Its smoothed daily evolution further indicates minimum influences (i.e., ''self-contamination'') of the previous stages of the diagnosed systems on the $\overline{[Z500]}$ values.

The maximum latitude of the subtropical belt defines its poleward edge, which varies for each hemisphere, day, and longitude of the analyzed period. The zonal mean of these latitudes is LAT_{MIN} (Fig. 1), which provides a simple hemispheric average of the location of the subtropical belt edge, and is herein taken as the minimum latitude for the occurrence of subtropical ridges and blocks. LAT_{MIN} is therefore defined for each day, as the latitude where the zonally averaged Z500 equals the subtropical belt threshold $\overline{[Z500]}$. Figure 3 shows the climatological annual cycle of LAT_{MIN} for both hemispheres and its interannual variability. LAT_{MIN} moves poleward from winter to summer in the corresponding hemisphere, therefore capturing seasonal variations associated with insolation, and hemispheric asymmetries (slightly larger seasonal migrations of the subtropical belt edge in the NH). The seasonal cycle of LAT_{MIN} remains quite stable along the reanalysis period, as shown by the relatively small spread, which reflects interannual

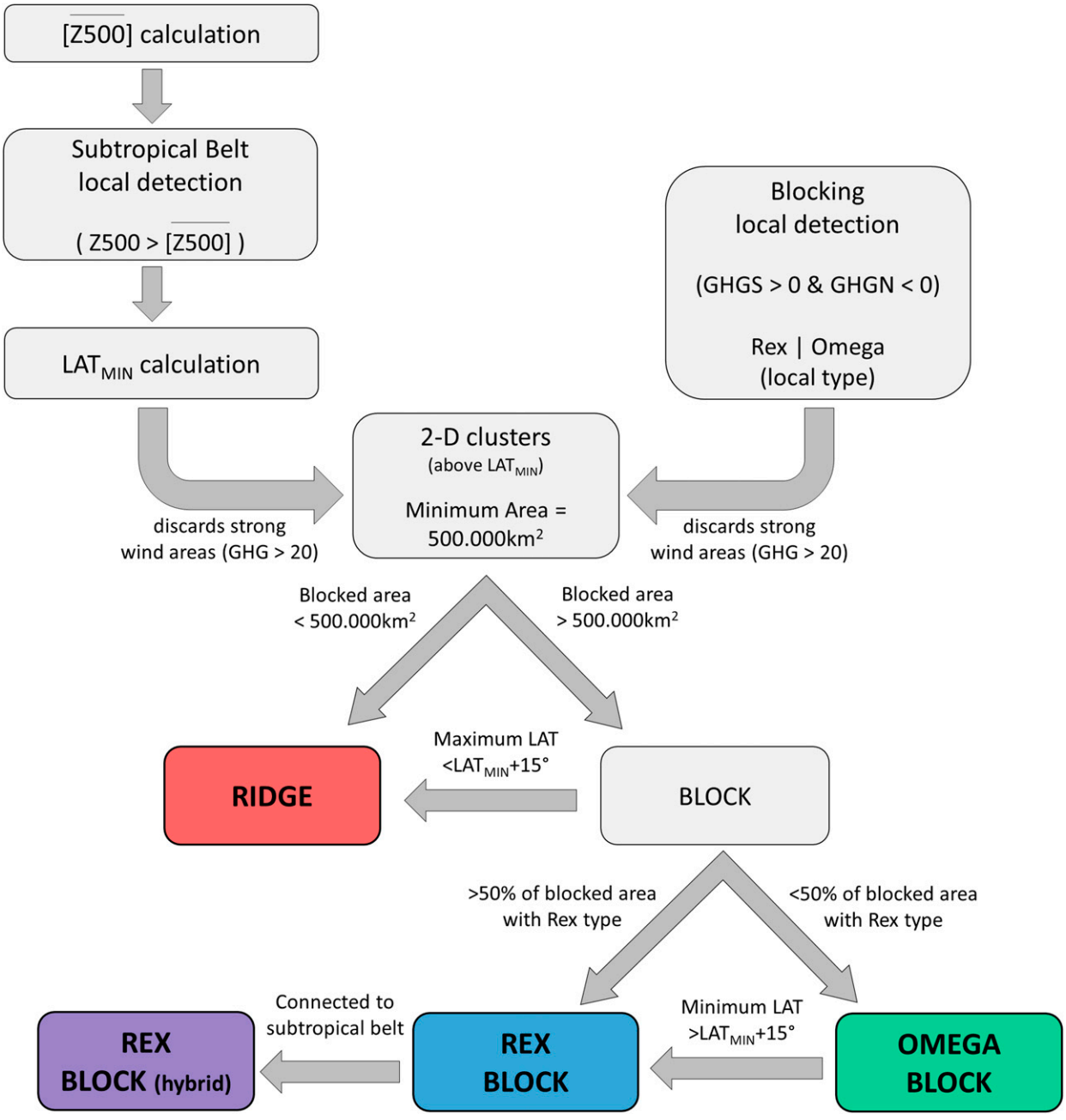

FIG. 2. Flowchart illustrating the sequence of steps and criteria employed from the local detection to the classification of 2D structures as ridges, omega blocks, and Rex blocks. See text for details.

(e.g., ENSO) and longer variations. NCEP–NCAR and ERA-5 datasets yield consistent LAT_{MIN} climatologies over their common period (1980–2020; Fig. S2). These results support the robustness of LAT_{MIN}, which also agrees well with other indicators of the subtropical belt edge, such as the averaged latitude of maximum Z500 meridional gradient (i.e., the subtropical jet; not shown). At this stage, all grid points embedded in the subtropical belt and extending poleward of LAT_{MIN} are considered local and instantaneous subtropical ridges (Fig. 2), while those detected equatorward of LAT_{MIN} are disregarded in subsequent analyses.

d. Local blocking detection

To detect local and instantaneous blocking, we use the extended 2D version of the Tibaldi–Molteni index, hereafter TM2D (Tibaldi and Molteni 1990), similar to that of Davini et al. (2012), with minor modifications. This procedure computes geopotential height gradients of Z500 and identifies

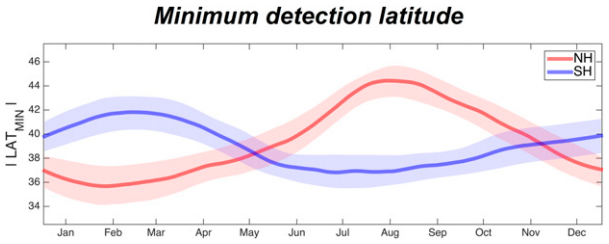

FIG. 3. Climatological (1950–2020) daily mean position of the subtropical belt edge (LAT_{MIN}; in degrees of latitude) for each hemisphere (colored lines). Shading shows the ±1 sigma interval for each calendar day (i.e., interannual and longer variations). Data source: NCEP–NCAR reanalysis.

individual blocked grid points based on the occurrence of meridional flow reversals (see also Fig. 2):

$$\text{Blocked: } \mathrm{GHGS}_{(\lambda,\phi,d)} > 0 \quad \text{and} \quad \mathrm{GHGN}_{(\lambda,\phi,d)} < 0, \tag{2}$$

with

$$\mathrm{GHGS}(\lambda,\phi,d) = \frac{[\mathrm{Z500}(\lambda,\phi,d) - \mathrm{Z500}(\lambda,\phi-\Delta\phi,d)]}{\Delta\phi} \quad (\text{if } \mathrm{LAT_{MIN}} \le \phi), \tag{3}$$

$$\mathrm{GHGN}(\lambda,\phi,d) = \frac{[\mathrm{Z500}(\lambda,\phi+\Delta\phi,d) - \mathrm{Z500}(\lambda,\phi,d)]}{\Delta\phi} \quad (\text{if } \mathrm{LAT_{MIN}} \le \phi \le 75°), \tag{4}$$

where λ, ϕ, and d follow the notation of Eq. (1) and $\Delta\phi = 15°$ (a typical latitudinal extension of blocking). GHGS and GHGN represent the occurrence of equatorward easterlies (flow reversals) and poleward westerlies with respect to the local blocked grid point, respectively. GHGS is computed for latitudes poleward of LAT_{MIN} (except $\phi = 90°$). This permits local grid points previously classified as ridges to become reclassified as blocks, therefore accounting for subtropical ridges that develop local wave breaking. Herein, the GHGN condition is not required for latitudes poleward of 75° (hereafter polar latitudes), where GHGN is undefined. For simplicity, local flow reversals at latitudes higher than 75° will also be considered blocks, but referred to as "polar blocks" in the following sections, to distinguish them from "canonical blocks" satisfying GHGS and GHGN conditions. For the remaining latitudes, the GHGN threshold has been relaxed as compared to that in the original TM2D method (GHGN < -10 m per degree) to avoid filtering local reversals that may occur far from the poleward westerlies in meridionally extended structures. This is also aligned with recent recommendations to progressively decrease the GHGN threshold with latitude (up to 0 m per degree for latitudes higher than 60°) in order to account for the weaker poleward westerlies associated with high-latitude blocks (Tyrlis et al. 2021). In the TM2D method, strong poleward westerlies were also required to ensure that the flow reversal is caused by a blocked high, therefore minimizing the detection of deep cutoff lows, which can cause large-scale easterlies in their poleward flanks. This and other potential misdetections will be treated separately in subsequent steps of the method.

Next, the TM2D method is further extended to distinguish between Rex and omega blocks. The rationale is illustrated in Fig. 4. It relies on the presence of strong westerlies equatorward of Rex blocks due to the southern branch of the associated split flow, which is absent in omega blocks. The so-diverted jet develops in the equatorward flank of the accompanying cut-off low, and hence can be diagnosed by

$$\mathrm{GHGS}_2(\lambda,\phi,d) = \frac{[\mathrm{Z500}(\lambda,\phi-\Delta\phi,d) - \mathrm{Z500}(\lambda,\phi-2\Delta\phi,d)]}{\Delta\phi}. \tag{5}$$

For a dipole-like Rex block, the meridional Z500 gradient maximizes immediately south of the blocking high (GHGS > 0) and reaches large negative values (i.e., strong westerlies) farther south (Fig. 4b). Differently, omega blocks (Fig. 4a) exhibit a smoother latitudinal variation of meridional Z500 gradients, with weaker reversals and equatorward westerlies (i.e., smaller differences between GHGS and $GHGS_2$) than Rex blocks. As a consequence, local and instantaneous blocking detection can be categorized as Rex or omega flows, as follows:

$$\text{Rex block: } \mathrm{GHGS}_{(\lambda,\phi,d)} - \mathrm{GHGS}_{2(\lambda,\phi,d)} > 20\,\text{m per degree}, \tag{6}$$

$$\text{omega block: } \mathrm{GHGS}_{(\lambda,\phi,d)} - \mathrm{GHGS}_{2(\lambda,\phi,d)} \le 20\,\text{m per degree}, \tag{7}$$

where the adopted threshold follows previous studies to diagnose strong zonal flows, as opposed to blocking conditions (e.g., Trigo et al. 2004; Sousa et al. 2017). Note that our approach can identify local omega and Rex classifications along the same meridian within individual contiguous structures. In this case, and for a particular structure (the clustering technique is detailed in section 2f), all blocked grid points of that longitude are classified as Rex. Visual inspection of selected cases confirmed that this circumstance tends to occur when the characteristic low pressure systems of Rex blocks are already present and growing equatorward of the blocking high.

e. *Local spatial filtering*

The local approaches can detect unwanted features, which mainly occur in jet structures surrounding ridges, blocks, and eventually cutoff lows. Therefore, we next try to remove spurious local detections of ridges and blocks by keeping only grid points embedded in the high pressure systems. The designed filter (Fig. 2) simply excludes from the detection those areas with strong flows, defined as

$$\mathrm{GHG}(\lambda,\phi,d) > 20\,\text{m per degree}, \tag{8}$$

where GHG represents a local measure of the geostrophic wind magnitude (wind module), with the wind components inferred from zonal and meridional Z500 gradients. These gradients are calculated using centered differences of $\Delta\phi/2$ width in longitude and latitude, respectively. The specific threshold for strong flows [the same as in Eqs. (6) and (7)] is not

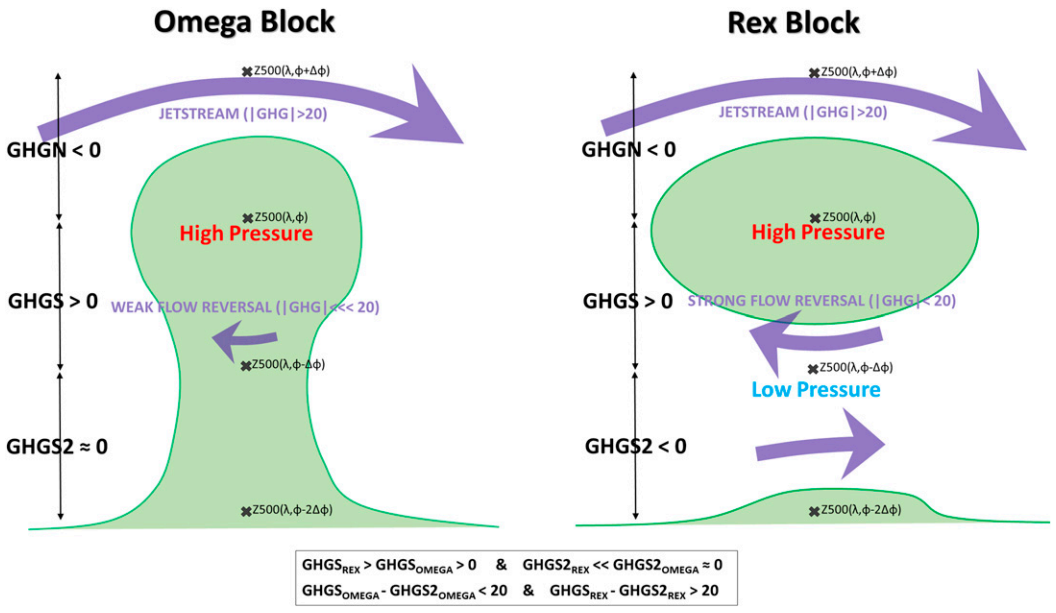

FIG. 4. Schematics of idealized omega and Rex blocks (as orientated in the NH), and the associated circulation and criteria employed for the classification of local blocking detections. Green shading represents areas of high pressure contoured by a representative isohypse. Arrows indicate zonal flows (strong westerly jets and easterlies). Crosses show the grid points (at distances of $\Delta\phi = 15°$) used in the computation of the meridional Z500 gradients (GHGN, GHGS, and $GHGS_2$) for a representative longitude.

critical for the method and retrieves a cleaner detection that will assist us in the identification and spatial separation of 2D structures (as exemplified in Fig. S3).

f. Instantaneous 2D structures

After the local and instantaneous detection of ridge/blocking, spatially contiguous grid points poleward of LAT_{MIN} are grouped into the same set, irrespective of their local classification (Fig. 2). Recall that the subtropical belt edge displays zonal asymmetries, and hence intrusions of the subtropical belt into the midlatitudes appear as isolated clusters poleward of LAT_{MIN}. Furthermore, the filter of Eq. (8) contributes to identify well-separated 2D structures by delimiting the boundaries of high pressure systems, and minimizes the occurrence of structures extending over all longitudes of a given hemisphere. For each day, only large-scale clustered structures with at least 500 000 km^2 of areal extent are retained. This threshold has also been employed in other TM2D methods as a minimum extension of flow reversals and assumes appreciable latitudinal scales (~5°) for midlatitude Rossby wave breaking over the typical longitudinal scales of blocking (~10°). It also provides an additional constraint to remove spurious small-scale systems (e.g., cutoff lows) that may have passed the filter of Eq. (8).

A given pattern can comprise grid points classified in different structures, which is useful for detailed dissections of the pattern, but impractical for climatological applications. Therefore, the entire structure is subsequently classified under the same type. The categorization of 2D structures into blocking or ridge does not rely on the simple balance of their areas. This approach would be detrimental to blocking because its areal estimates only account for the extension of flow reversals, which do not necessarily extend over the full high pressure. Therefore, the classification of 2D structures uses blocking-related areal criteria (see Fig. 2), which are better established and avoid biases from inaccurate estimates of ridges' extension:

1) Subtropical ridge (red box in Fig. 2)—This term applies if less than 500 000 km^2 of the total area is blocked or the structure extends less than $\Delta\phi = 15°$ in latitude poleward LAT_{MIN} (Figs. 1a,b). Otherwise, the structure is classified as a block and conditions 2a and 2b are evaluated.

2a) Omega block (green box in Fig. 2)—This term applies if more than half of the blocked area is detected as omega and the structure is close enough to subtropics (no farther than $\Delta\phi = 15°$ from LAT_{MIN}) (Fig. 1c).

2b) Otherwise (i.e., if point 2a is not satisfied), the block is considered Rex (Figs. 1d,e).

According to definition 1 above, blocks must exhibit appreciable meridional extensions (at least $\Delta\phi = 15°$) from LAT_{MIN} and Rossby wave breaking on synoptic or larger spatial scales (at least 500 000 km^2 of blocked area), in agreement with the conceptual model. Similarly, the second condition in definition 2a was included to emphasize subtropical links with omega blocks, following the conceptual model, but it was not critical (less than 5% of global blocks affected). Therefore, the categorization of blocks largely depends on whether the area of flow reversal is dominated by omega or Rex flows. As stated above, Rex blocks admit a subtype classification into Rex-pure and Rex-hybrid. The latter is said to occur if the Rex block reaches LAT_{MIN} so that it is not detached from

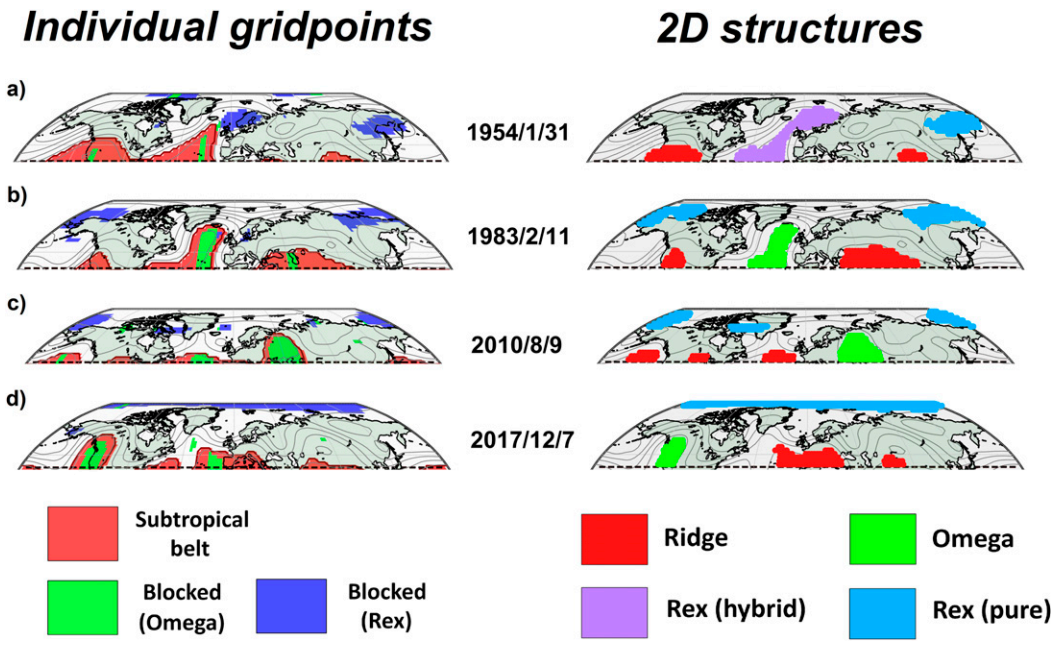

FIG. 5. Examples of the local and instantaneous detection scheme and identification of 2D structures. (left) Individual classification of grid points as subtropical ridge or block types (omega or Rex). (right) The type of system assigned to each isolated 2D structure exceeding the minimum areal extent criterion (red: subtropical ridge; green: omega block; purple: Rex-hybrid block; blue: Rex-pure block). The dashed line shows the minimum detection latitude (LAT_{MIN}) for that specific date. Black contours depict the daily Z500 field (in 150-m intervals). Data source: NCEP–NCAR reanalysis.

the subtropical belt (Fig. 1d; purple box in Fig. 2). Otherwise, the Rex block is simply considered Rex-pure (Fig. 1e; blue box in Fig. 2). According to this classification, polar blocks are included in the (pure) Rex category, as they are located poleward of 75°. However, we will keep the term ''polar blocks'' when referring to these structures and treat them separately when possible to stress the fact that they simply reflect large-scale flow reversals in polar regions and not necessarily classical blocks.

Once the full 2D structure is classified in one of these categories, all embedded grid points are labeled as such. Some examples of the local and instantaneous classification and subsequent identification of 2D structures are shown in the left and right panels of Fig. 5. For completeness, Fig. 5 also distinguishes the subtypes of Rex blocks. Note that subtropical ridges that do not reach large meridional extensions can exhibit wave breaking (cf. the structure over western Europe in the bottom panels of Fig. 5). Similarly, blocking can be well connected to the subtropical belt (e.g., the omega block over western North America in the bottom panels of Fig. 5). This multifaceted view of patterns reflects the commonly observed mixture of structures and provides a flexible approach for better treatment of transitions and tracking of evolving patterns.

g. *Tracking procedure and identification of events*

After the classification of individual structures, a spatio-temporal tracking algorithm is applied to identify persistent events and characterize their life cycles. Two structures of any type occurring in successive days are considered the same event if they have at least 50% of their areas in common. In the case that more than one structure satisfies this condition, the algorithm chooses the one with the largest overlap. This threshold has also been employed in other blocking methods [see, e.g., the three blocking indices in Woollings et al. (2018)] and was preferred over restrictive quasi-stationarity to account for the more transient nature of subtropical ridges and changes in the spatial pattern of the 2D structures during their transitions. A minimum duration criterion of four days is applied for the consideration of events, in overall agreement with previous studies of ridges and blocks (e.g., Barriopedro et al. 2010; Sousa et al. 2018a). Daily structures that do not form an event with the minimum duration are discarded. Note that the daily patterns of a given event may be of different type during its life cycle, allowing us to explore its daily transitions. However, for simplicity, the overall event will be referred to as ridge/omega/Rex (the latter being pure or hybrid) according to the most frequent type of structure during its life cycle. In case of equal frequency of daily structures, preference is given to patterns representing mature stages in our conceptual model (i.e., Rex blocks, followed by omega blocks and ridges).

In summary, the method provides a 3D array containing the daily occurrences and types of 2D structures conforming to the events. This product is complemented with a catalog of events, which lists the type and duration of the events and their mean characteristics as inferred by averaging some daily parameters

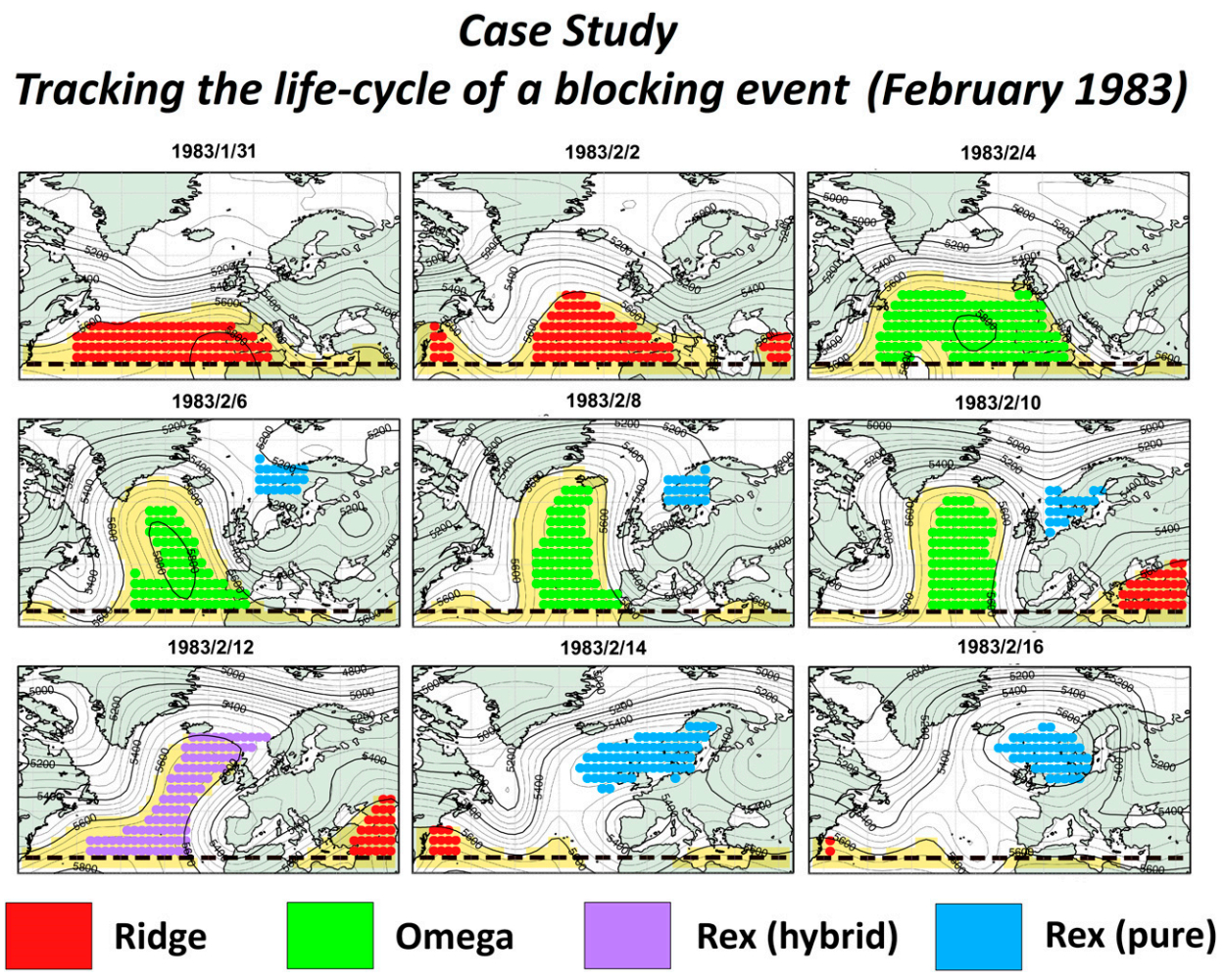

FIG. 6. Example of the life cycle of a blocking event during February 1983. Colored circles identify the daily 2D structures detected during the event, with the color code representing the type of pattern (red: subtropical ridge; green: omega block; purple: Rex-hybrid block; blue: Rex-pure block). Yellow shading depicts the areas embedded in the subtropical belt. Black contours represent Z500 (in 50-m intervals) and the dashed black line shows the minimum detection latitude for each day (LAT_{MIN}). Data source: NCEP–NCAR reanalysis.

(e.g., mean location, areal extent) over the life cycle. Obviously, changes in the above criteria (e.g., the minimum areal extent of the 2D structures, duration, etc.) affect the frequencies of the detected events. However, reasonable thresholds' variations tested during the process yielded comparable effects in all types of events and hence similar climatological distributions (e.g., preferential areas of occurrence, relative frequencies of events, etc.).

h. Case study: Tracking the life cycle of a blocking event

To better illustrate the methodology and catalog, we present a case study of a blocking event that occurred in the winter of 1983 over the northeastern Atlantic. This episode caused outstanding cold conditions over western Europe, including one of the most notable snowfall events in Iberia (11–15 February 1983). The event originated from a subtropical ridge over the northeastern Atlantic in January, during which it only experienced brief phases as a shallow omega block (not shown). Figure 6 shows the daily structures that conform the event (colored circles) during the period spanning 31 January–16 February 1983. By early February the subtropical ridge (red) gradually stretched to the north, and eventually overturned over a widespread area, thus transitioning to an omega block (green). During this phase, the block displayed pronounced overturning on both sides of the block and remained relatively stationary for around one week, reaching latitudes close to Iceland. By 12 February, the structure presented Rex-like characteristics, although still partially connected to the subtropical belt (Rex-hybrid block; purple). This pronounced tilt (anticipating a complete breaking) was accompanied by a deep low pressure system in the southeastern flank of the block. In the following days the blocking high detached completely from the subtropics, and remained as a dipole-like Rex block (Rex-pure; blue) at higher latitudes until 21 February.

In Fig. S4, two additional examples are provided. The first one (Fig. S4a) illustrates the typical life cycle of a ridge event in

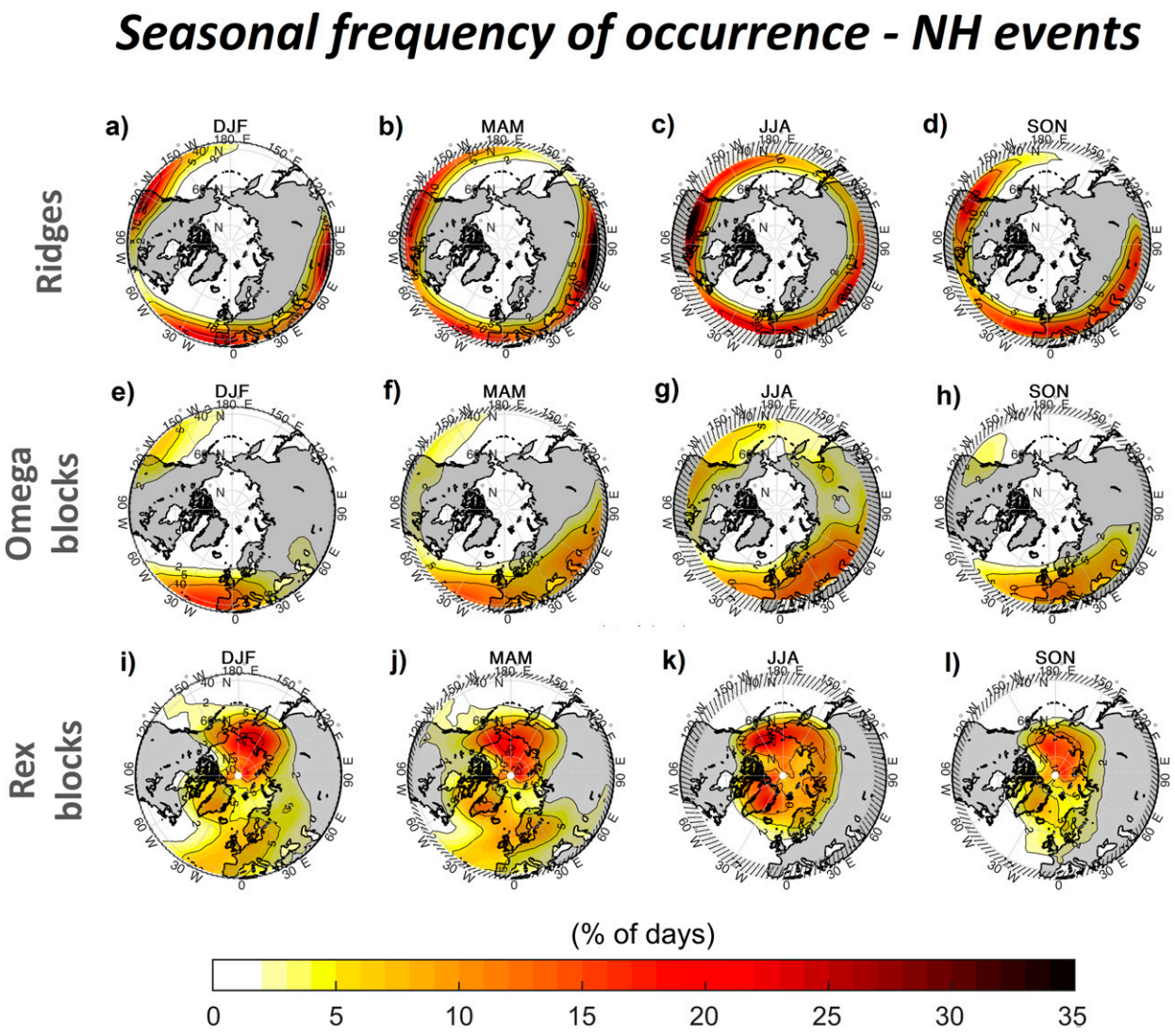

FIG. 7. Climatological mean (1950–2020) seasonal frequency of occurrence of subtropical ridge events in the NH (in percentage of seasonal days) for (a) DJF, (b) MAM, (c) JJA, and (d) SON. (e)–(h) As in (a)–(d), but for omega block events. (i)–(l) As in (a)–(d), but for Rex block events. Results are only shown for areas poleward of the averaged minimum detection latitude (LAT_{MIN}). Note that events of a given type can include daily structures of different types. Polar blocks are included in the Rex-block category. Data source: NCEP–NCAR reanalysis.

the SH. Due to the dominant zonal flow, as compared to that of the NH, wave breakings are much more limited spatially and temporarily therein, resulting in frequent back-and-forth transitions to subtropical ridges and lower occurrence/persistence of midlatitude blocks, as shown in this example. The final example (Fig. S4b) illustrates the occurrence of summer ridge/blocking activity over North America, and the ability of the method to discriminate events that occur at different latitudes of the same sector.

In summary, these case studies demonstrate that the proposed methodology can capture the spatial patterns and complex transitions of quasi-stationary high pressure systems with large impacts on both subtropical and extratropical latitudes. They also stress the limitations of previous systematic approaches, which have mainly focused on blocking only, disregarding the crucial role of subtropical ridges in the onset, development (e.g., transitions with omega blocks), and decay of mature Rex blocks. The next section presents the first global climatology of subtropical ridges and blocking event types.

3. Climatology

a. Spatial distribution of events

Herein, we used the catalog of events to identify all subtropical ridge, omega block, and Rex block events of 1950–2020. Then, all daily 2D structures that conform to each event were extracted from the 3D product. Figures 7 and 8 show the

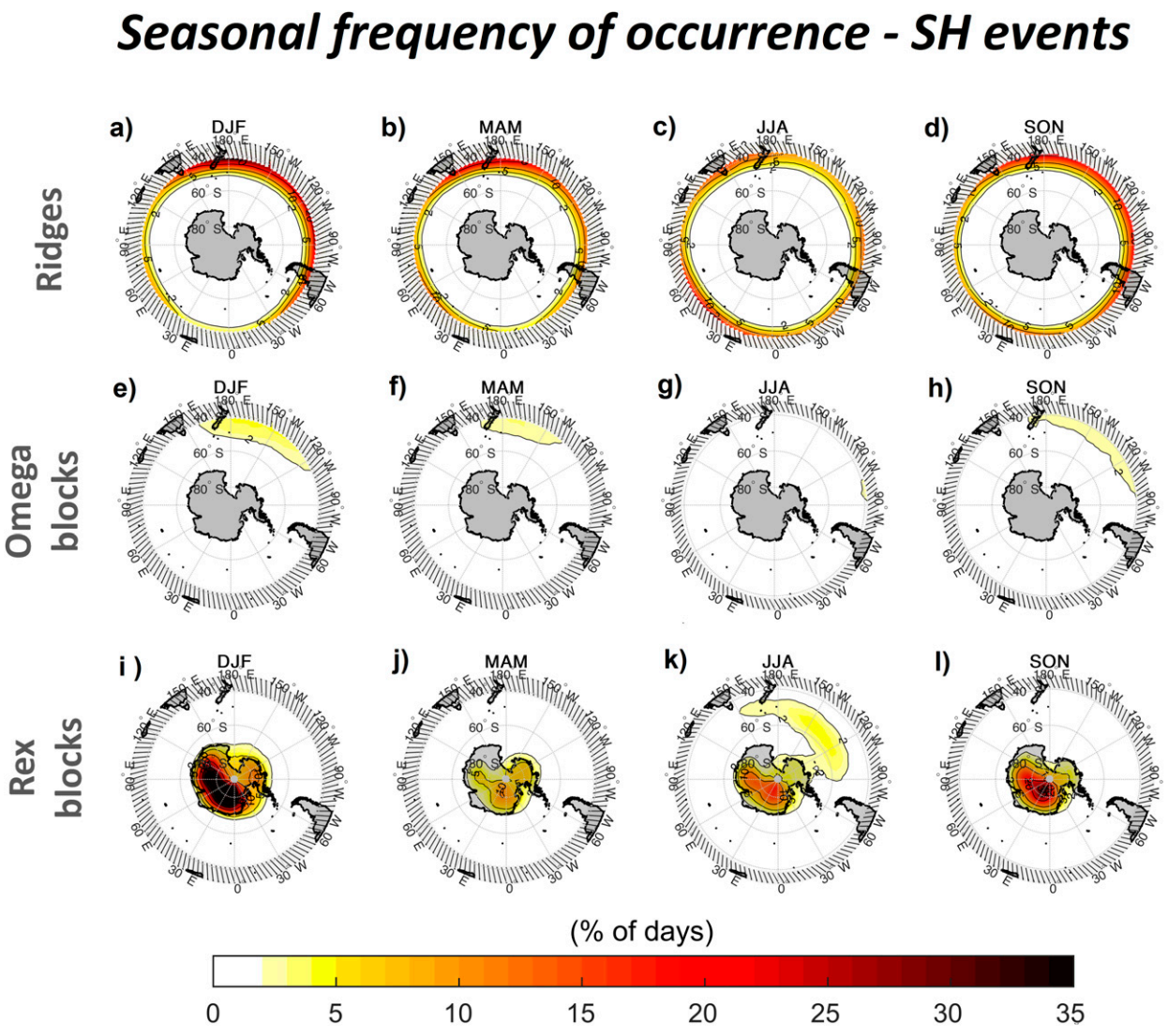

FIG. 8. As Fig. 7, but for the SH.

seasonal maps with the mean frequency of occurrence of these events for the NH and SH, respectively, following the conventional notation of seasons [e.g., December–February (DJF) for the boreal winter/austral summer].

Subtropical ridge events are common in the NH through the year, and tend to occur over climatological regions of Rossby wave amplification (e.g., the eastern sides of the Pacific and Atlantic Oceans). Midlatitude areas of western Europe, central Eurasia, and western North America are the preferential areas for subtropical ridge occurrence, with frequencies well above 10% all year round (Figs. 7a–d). These events are more frequent (~20%) during the warmer months, when they migrate poleward. Areas that are seasonally or annually embedded in the subtropical belt (i.e., equatorward of LAT_{MIN}) become subject to the permanent high pressure regime of the subtropics and, by definition, do not experience temporary intrusions of the subtropical belt, being therefore masked (e.g., the Mediterranean during summer; Fig. 7c).

There are marked differences in the NH spatial distribution of omega (Figs. 7e–h) and Rex (Figs. 7i–l) events. Omega blocks preferentially occur at lower latitudes of the eastern oceanic basins, in close agreement with regions of subtropical ridge incidence. This is notable in western Europe and North America, where subtropical ridges and omega blocks are present all year round, locally accounting for up to one-third of seasonal days. This suggests that persistent poleward extended ridges cannot be maintained without wave breaking in these regions, with the possible exception of eastern Asia, where the spatial match of these events is less evident.

NH Rex blocks are essentially located at high latitudes, particularly in the sectors between Greenland/Scandinavia and Siberia/Alaska, and are more common in winter and spring, in line with previous blocking climatologies (e.g., Barriopedro et al. 2006; Masato et al. 2012). Rex blocks can reach polar latitudes, although these structures do not often block the eddy-driven jet stream (e.g., eastern Asia; Barriopedro et al. 2010).

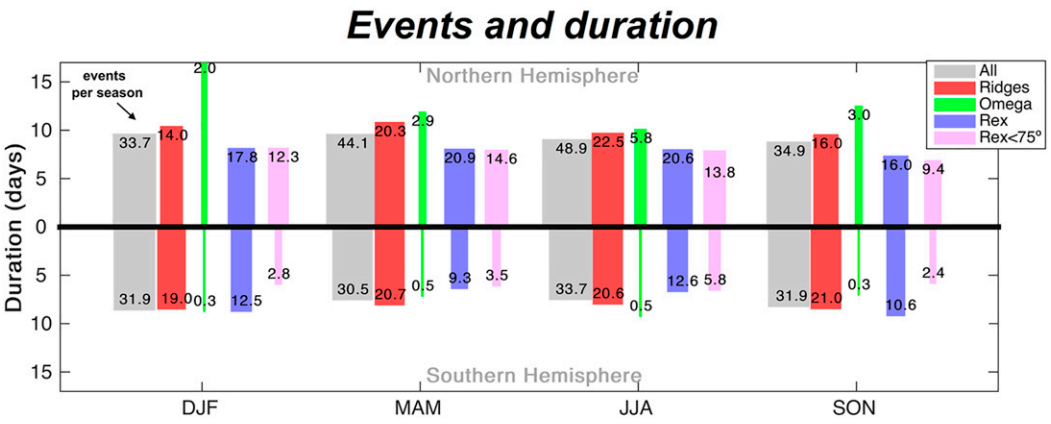

FIG. 9. Seasonal mean (1950–2020) duration (days; bar height) and frequency of occurrence (bar width and black numbers) of events classified as subtropical ridges (red bars), omega blocks (green bars), and Rex blocks (blue bars). Pink bars show the corresponding values for Rex blocks equatorward of 75°, therefore excluding polar events. Gray bars correspond to all events, regardless of their type. Diagnostics for the NH and SH events are shown in the upper and bottom half of the plot, respectively. Data source: NCEP–NCAR reanalysis.

There are also appreciable frequencies of occurrence near the subtropics (e.g., the eastern Atlantic), in particular during winter and spring (Figs. 7i,j). They largely correspond to Rex-hybrid events (shown in Fig. S5), which often exhibit subtropical connections and temporary stages of omega blocks (e.g., the case study of Fig. 6). These block events are relatively less frequent over the eastern Pacific, this interbasin asymmetry being likely due to the more tilted jet stream and higher frequency of anticyclonic wave breaking over the eastern Atlantic (e.g., Masato et al. 2012). A clearer detachment of Rex blocks from the subtropical belt can also be observed in all regions during boreal summer and autumn (Figs. 7k–l).

The analysis for the SH shows striking differences when compared to the NH. Subtropical ridge events are also relatively frequent in the SH, but the spatial distribution is more zonally symmetric, and the poleward summer migration is smaller than in the NH (Figs. 8a–d). Midlatitude excursions of the subtropical belt are more frequent in the Pacific and Indian Oceans. The Pacific Ocean is also the preferred sector for omega (Figs. 8e–h) and winter Rex (Fig. 8k) events. This is in agreement with previous studies of SH blocking (e.g., Berrisford et al. 2007; Dong et al. 2008). However, we find comparatively lower frequencies (~5%) because structures that were considered blocks in those studies fall here within the subtropical ridge category, according to our conceptual model. In fact, persistent blocking patterns are very rare in the midlatitudes of the SH, and they most commonly manifest during short periods before dissipating, or as temporary phases of subtropical ridge events (e.g., case study 2 of Fig. S4). This suggests that a substantial part of the blocking events considered in previous works is sporadic manifestations of longer-lasting intrusions of the subtropical belt. This is not surprising, considering the dominance of oceanic areas in the SH, which supports a less perturbed zonal flow, and low frequencies of wave breaking (Peters and Waugh 2003; Ndarana and Waugh 2011). Differently, Rex-like events are common in polar areas of the SH (so-called polar blocks), particularly over the eastern plateau of Antarctica during the austral summer (Fig. 8i). These semipermanent Antarctic systems do not fit into the conceptual model of midlatitude wave breaking and associated weakening of the jet stream (Fig. 1). Preliminary analyses based on composites of regional polar blocks (Fig. S6 in the online supplemental material) support the Rex-like pattern of these structures, with high pressure anomalies over the Antarctica bounded by deepened lows at equatorward latitudes (in the poleward flank of the jet). However, and similar to other structures termed blocks (e.g., "low-latitude blocks"), these patterns involve strong westerlies at the jet latitudes. Therefore, they should not be viewed as classical blocks but rather as a different family of flow-reversal events, likely associated with persistent episodes of polar easterlies over Antarctica. Wave activity in this polar region has been reported in previous studies and considered a key mechanism to extract the westerly momentum generated by drag of the surface easterlies at the slopes of Antarctica (Egger 1985). However, additional studies are required to elucidate the physical processes associated with polar blocks and the extent to which these structures can be considered blocking-like patterns.

By disentangling subtropical ridges and blocks, our results help reconcile some distinctive features of previous studies that contribute to the disparity of blocking climatologies in regions of both hemispheres. They include the low-latitude blocks of the NH (Davini et al. 2012) and the relatively high frequency of midlatitude SH blocking (Mendes et al. 2008) and persistent Z500 maxima (Liu et al. 2018), which could rather reflect structures of essentially subtropical characteristics. Finally, we note that the climatological frequencies of events are very similar in the two reanalyses for their common period (1980–2020), except over Antarctica, where polar blocks are ~10% more frequent in ERA-5 and show slightly different spatial distributions during austral summer and autumn.

b. *Duration and life cycle transitions of events*

The preferential regions for high pressure systems shown in Figs. 7 and 8 can result from recurrent events, long persistence of events, or both. This question is addressed in Fig. 9, which

shows the mean duration of events (bar height) along with the total frequency of event occurrence (bar width/numbers) for each season and hemisphere. The analysis is performed for all events (gray bars) and each type of event (color bars). Due to the different nature of polar blocks and the reanalyses' discrepancies in Antarctic blocks, we also consider canonical (i.e., nonpolar) Rex block events separately.

Overall, the total number of events is higher in the NH than in the SH (~160 vs ~120), and the mean duration is also higher (~9 days in the NH, and ~7 days in the SH), despite some seasonal differences. Subtropical ridges are the most frequent events in the NH during summer, whereas Rex blocks are during other seasons. Overall, all events tend to be slightly shorter-lived during summer. This is in agreement with more transient features, arising from weaker stationary waves and probably also eddy feedback, which are needed to support long-lasting events (e.g., Drouard and Woollings 2018). Omega blocks (green bars in Fig. 9) present the longest durations of all NH events (~16 days in winter and ~10 days in summer), but this result could be affected by the small sample size (less than four events per season, on average). Indeed, omega blocks are relatively uncommon as full events, as they commonly represent intermediate stages between subtropical ridges and mature Rex blocks (e.g., Fig. 6). Despite the low frequency of omega events, the number of days affected by these events is comparable to that of Rex blocks (cf. Figs. 7e–h and Figs. 7i–l), stressing the major contribution of omega blocking persistence to the seasonal frequencies of occurrence. Finally, we note that most NH Rex blocks correspond to nonpolar events, therein including those associated with persistent cold anticyclones over northeastern Eurasia (Cheung et al. 2013; Antokhina et al. 2017).

In the SH, the characteristics of Rex block events are largely dominated by those occurring over Antarctica. When polar blocks are not considered in the statistics, the seasonal frequency of Rex events reduces significantly, thus reinforcing the very transient nature of wave breaking and canonical block events in the SH. Similar to the NH, subtropical ridges represent the most frequent type of events in the SH, although the difference with midlatitude blocks is comparatively larger than for the NH, due to the low occurrence of the latter in the SH. This again supports the shallower and/or more transient characteristics of SH nonpolar blocks, which frequently appear as temporary stages of other types of events rather than as isolated events. The eddy activity over Antarctic orography may favor polar blocks, and eventually disfavor nonpolar blocks, due to its crucial role in maintaining the strong SH midlatitude jet stream (Patterson et al. 2020).

To analyze in more detail the life cycle of events, we considered the classification of the daily 2D structures that conform to the events of the catalog. By that means we identified the transitions between ridges and block patterns along the life cycle of all events, as well as their locations of occurrence (i.e., mean longitude and latitude of the daily 2D structure transitioning to a different pattern). Figure 10 maps the preferred phase transitions for each hemisphere and season. As a substantial fraction of the events are first detected as subtropical ridges, we also show the location of these subtropical ridges (red circles), therefore indicating the overall onset location of events.

The comparison between the NH and SH shows striking differences for all seasons. While phase transitions are common over widespread regions of the NH (Figs. 10a–d), many fewer occur in the SH (Figs. 10e–h), being largely confined to the Pacific, in agreement with the results described in section 3a. In the NH, a large fraction of subtropical ridges evolves into blocks (~50%, against only ~15% in the SH), particularly over the eastern oceanic basins and adjacent continents in winter, with a more dispersed distribution during summer. Overall, this distribution agrees with the preferential areas for wave breaking and blocking activity (e.g., Nakamura and Huang 2018). Coherent with the conceptual model, the mean latitude of NH transitions increases from ridge ↔ omega to omega ↔ Rex-hybrid and omega ↔ Rex-pure. Transitions involving Rex-hybrid blocks are largely confined to eastern Atlantic and western Eurasia, as aforementioned. Finally, summer blocks at very high latitudes (Fig. 10c) experience frequent transitions (from omega types), as compared to their winter counterparts. If transitions are viewed as a limiting factor for blocking persistence, this contrasting seasonal behavior would be in agreement with the more persistent and quasi-stationary behavior of winter polar blocks (Fig. 9). In the SH, instead, subtropical ridges tend to remain as such through most of their life cycle, with the exception of a few transitions to blocks, mainly over the Pacific and eastern Indian Oceans during the cold seasons (Figs. 10f,g). It is worth noticing that no transitions are detected over Antarctica, supporting that polar blocks likely reflect persistent regional processes that do not match with the typical life cycle of a block (midlatitude Rossby wave-breaking processes).

c. *Long-term trends in ridge and blocking frequency*

Special attention has been paid to recent changes in blocking activity (e.g., Barnes et al. 2014), partially motivated by suggested associations with Arctic amplification (e.g., Stuecker et al. 2018; Dai et al. 2019). Tropical/subtropical expansion (e.g., Staten et al. 2018) has also been a recurrent topic of active research, although to our knowledge there are no global studies dealing with trends in atmospheric systems associated with temporary regional poleward migrations of the subtropical belt. In this subsection, we analyze trends in the seasonal frequency of occurrence of events (section 3a) for the 1950–2020 period (Fig . 11) and compare them with recent changes for the common period (1980–2020) of NCEP–NCAR and ERA5 reanalyses (Fig. 12). Linear trends are based on zonal assessments, using the number of days in the season with at least one event at the given latitude, and expressed in percentage of decadal changes with respect to the climatological frequency. Further 2D details on the spatial distribution of trends, including those for each type of structure, can be found in Figs. S7 and S8 in the online supplemental material. To avoid eventual overstatements of changes in areas with low occurrence of events, trends that are not statistically significant (no hatching) and that are observed in areas with low climatological frequencies of occurrence (displayed by the black lines) should be considered with caution. Unless otherwise stated, the trends described here are consistent between reanalyses.

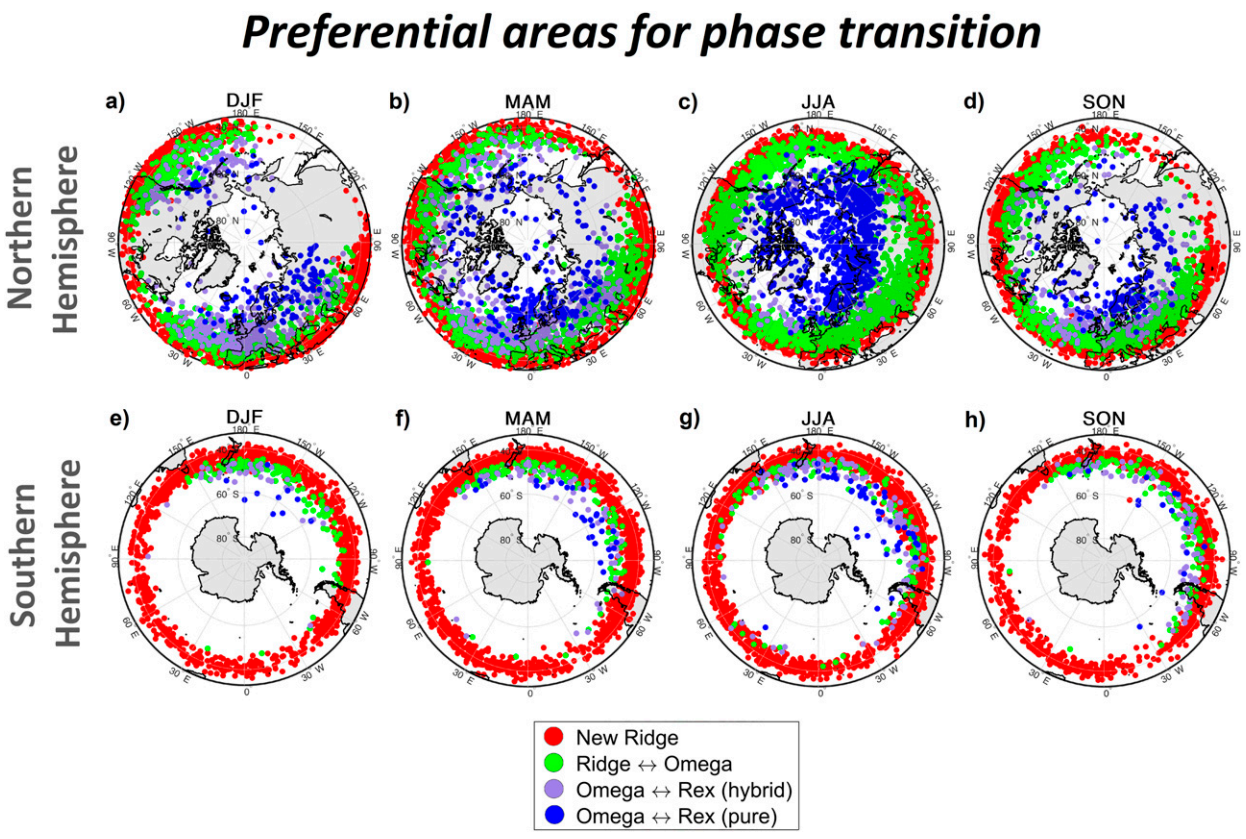

FIG. 10. Spatial locations of selected transitions between different types of daily patterns during the life cycle of all events (1950–2020) for (a) DJF, (b) MAM, (c) JJA, and (d) SON in the NH. (e)–(h) As in (a)–(d), but for the SH. Red dots depict the onset location of events starting as subtropical ridges. The remaining colored dots correspond to the spatial center of 2D daily structures experiencing transitions between subtropical ridge and omega block (green), omega block and Rex-hybrid block (purple), and omega block and Rex-pure block (blue). Results are only shown for areas poleward of the averaged minimum detection latitude (LAT_{MIN}). For better readability, we do not include all possible transitions. Data source: NCEP–NCAR reanalysis.

For the NH, there are no significant hemisphere-wide trends since 1950. Instead, latitudinal and seasonal opposing changes tend to dominate (Figs. 11a–c), which may be affected by large internal variability on regional scales and hence be susceptible to the analyzed period. Some notable features, often restricted to specific seasons, are (i) an increase in low-latitude events (<50°N) in spring; (ii) a decrease in midlatitude (50°–65°N) and high-latitude (65°–75°N) events, more pronounced in winter and summer, respectively; and (iii) a significant increase of polar events (>75°N), mainly in winter. Low-latitude increases are essentially driven by subtropical ridge events and secondarily omega blocks, while the small decreases over mid- and high-latitude regions reflect a tendency for reduced blocking occurrence. Long-term increases in blocking events are essentially restricted to polar areas. The spatial distribution of seasonal trends (Figs. S7a–d) further depicts zonally opposing trends, such as those over the eastern Atlantic and western Europe, which suggest an eastward displacement of low-latitude structures (ridges and omega blocks; Figs. S8a–h) toward the continent. However, the magnitude, significance, and/or sign of regional changes often differ when trends are computed for a shorter period (1980–2020; Figs. S7i–l), even for the zonal trends (e.g., polar trends in Figs. 11a and 12a), suggesting large influence of internal variability. Spatial trends in blocks do not draw a robust consistent picture, with decreases being overall more common in nonpolar regions (Fig. 11c) and regional increases dominating the high latitudes (e.g., summer Greenland blocking increases for 1980–2020; e.g., Hanna et al. 2016; Davini and D'Andrea 2020; Figs. S7j–k). The apparent long-term increase of low-latitude systems and slight decrease of nonpolar blocking activity may suggest enhanced meridional Z500 gradients, although we note that these trends are either nonsignificant or occur in different seasons (Figs. 11a–c). Therefore, our results prevent statements on NH generalized trends, and further support a complex pattern of regional changes. Some of these long-term regional trends (e.g., the winter eastward migration of low-latitude events in the Euro-Atlantic sector) are in agreement with previous assessments (e.g., Davini et al. 2012), as well as with future projections suggesting an otherwise uncertain narrowing and eastward extension of the North Atlantic jet (e.g., Peings et al. 2018). However, for the winter season addressed in these studies, we find that regional trends are not robust to the analyzed period (Figs. S7a,i). Our results do not point to statistically significant

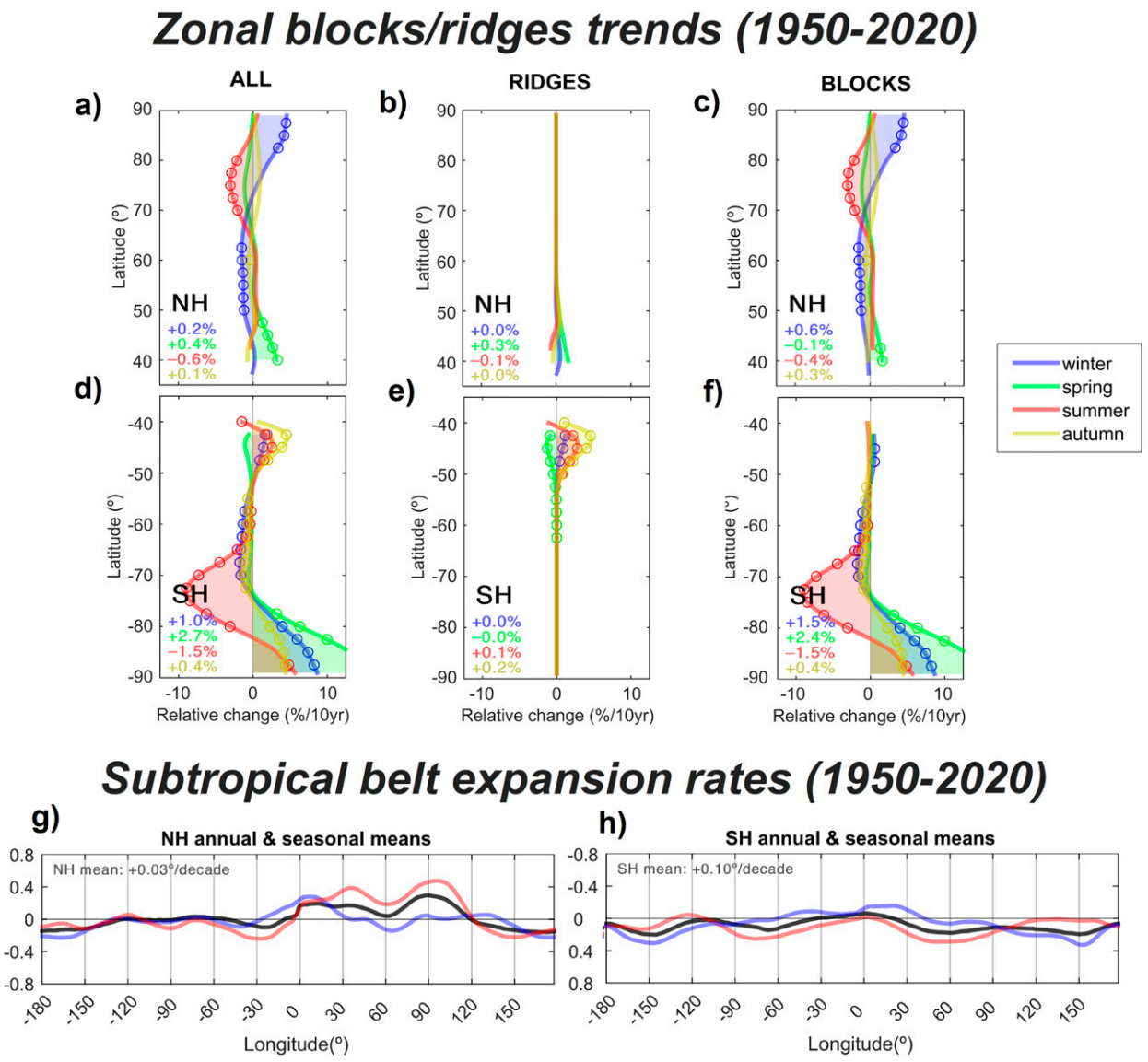

FIG. 11. (a) Seasonal trends (1950–2020, expressed as decadal changes with respect to the climatology) in the frequency of days with blocking and subtropical ridge events at each latitude of the NH. (b) As in (a), but for subtropical ridge events. (c) As in (a), but for blocking events (herein including polar events). (d)–(f) As in (a)–(c), but for the SH. Circles represent trends that are statistically significant at the 95% confidence level, after a Kolmogorov–Smirnov test. Hemisphere-wide trends are also shown in the left bottom corner of each panel. (g) Poleward trends (1950–2020, in degrees per decade) of the subtropical belt edge for each longitude (x axis) of the NH. Winter, summer, and annual averages are shown in blue, red, and black, respectively. The NH trend is also shown in the top left corner. (h) As in (g), but for the SH. Data source: NCEP–NCAR reanalysis.

midlatitude blocking increases during the recent period of Arctic amplification, as hypothesized in response to sea ice loss (e.g., Francis and Vavrus 2012) but in practice restricted to the Arctic, if they occur at all.

In the SH, the frequency of low-latitude events reveals long-term increases (except in spring), largely attributable to trends in subtropical ridges (Figs. 11d,e). These changes are more pronounced over the Pacific Ocean (Figs. S8m–p) and for the 1980–2020 period (Figs. 12d,e). There are also hints of long-term increases of subtropical ridge frequencies in the vicinity of South America (i.e., southeastern Pacific and southwestern Atlantic) in most seasons. These regional changes vaguely resemble the eastward migration of Euro-Atlantic events toward continental areas, but, as in that case, trends tend to weaken or vanish for the more recent period (cf. Figs. S7e–h and Figs. S7m–p). Nonpolar blocks show long-term decreases, particularly pronounced at high latitudes during austral summer, which are accompanied by increases of polar blocks near the South Pole (Fig. 11f). Although weaker, a significant declining trend in nonpolar blocks is also observed for the recent period and in both reanalyses (Fig. 12f). This consistency contrasts with that in Antarctic events, whose trends show marked

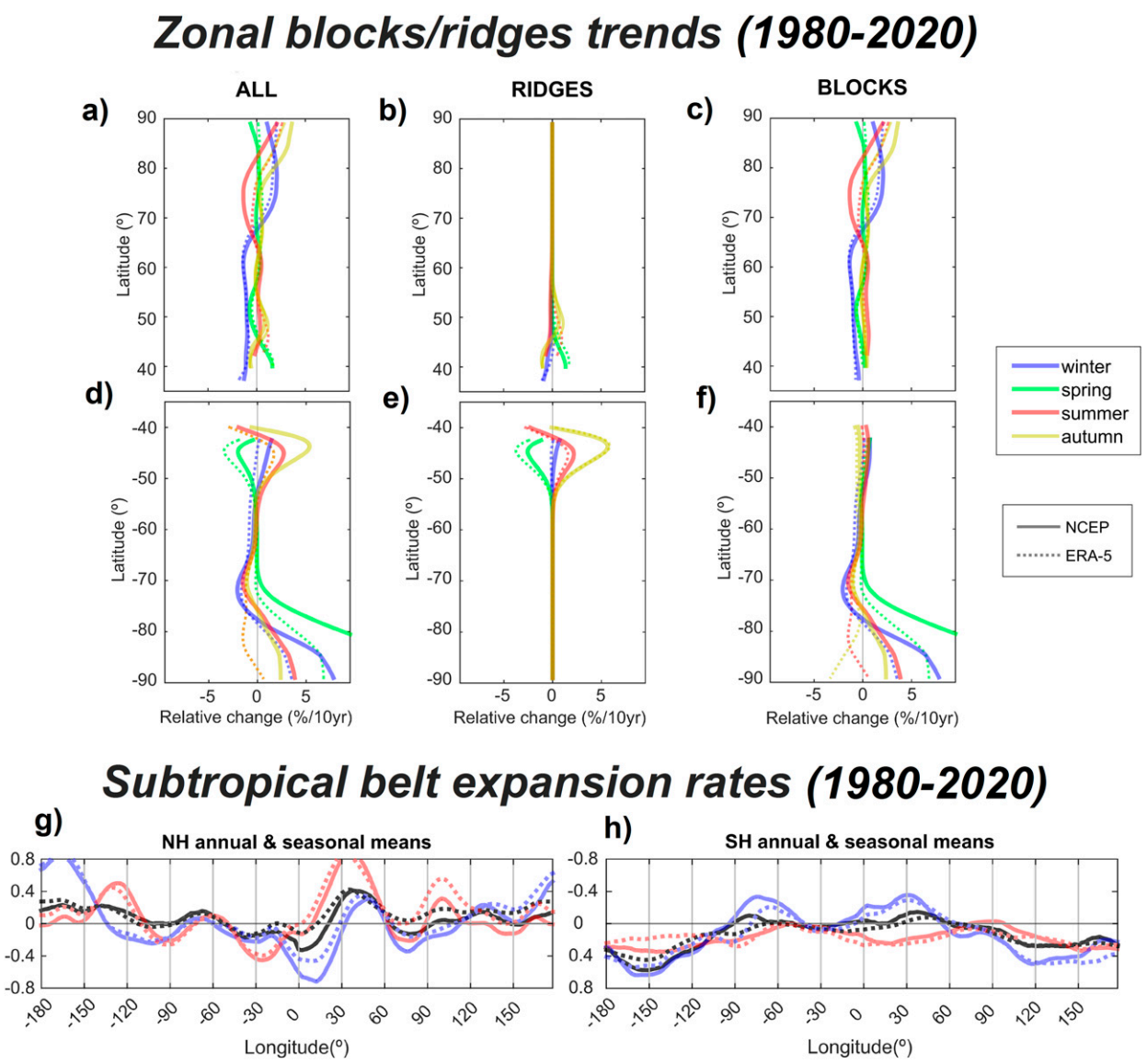

FIG. 12. As in Fig. 11, but for the common period (1980–2020) of NCEP–NCAR (solid) and ERA5 (dashed) reanalyses. For a clearer visualization, statistically significant trends and hemisphere-wide means are not shown.

discrepancies between reanalyses, further questioning the reliability of the reported changes in polar blocks for the longer period. The nonpolar blocking decreases agree with the strengthening of the westerly jet associated with the positive long-term trends in the southern annular mode (SAM), which are particularly pronounced during austral summer (Swart et al. 2015). Therefore, and obviating the more uncertain changes of polar blocks, zonally averaged trends in the frequency of SH events tend to depict larger and more sustained signals than those found for the NH.

d. Long-term trends in the subtropical belt edge

As described in section 2c, the detection method accounts for long-term changes in the subtropical belt edge (as diagnosed by LAT_{MIN}). Therefore, some of the abovementioned trends in events may reflect concurrent changes in the extension of the subtropical belt. To address this question, we computed monthly trends of the subtropical belt edge. Results show a generalized poleward expansion in the SH (Fig. 11h), with an all year-round shift of $+0.10°$ per decade ($p < 0.05$), thus corresponding to nearly a 1° change for the whole hemisphere during the 1950–2020 period. This agrees with recent assessments attributing the SH tropical expansion to increasing greenhouse gases and ozone depletion (Grise et al. 2019). The SH trend is more than doubled in certain sectors (e.g., those of semipermanent subtropical anticyclones) and particularly pronounced during the austral summer. Regional trends in the NH can be large and exceed those of the SH, although they are often masked on annual scales due to contrasting seasonal trends, therefore yielding a small mean poleward trend of $+0.03°$ decade^{-1} ($p < 0.10$). These results suggest that regional variability associated with

low-frequency variations may dominate NH trends in the subtropical belt edge, as has been reported for the tropical expansion of the NH (Grise et al. 2019). Regional and seasonal changes in the subtropical belt edge are larger in both hemispheres when considering only data since 1980 (Figs. 12g,h). Hemisphere-wide subtropical widening rates are also higher during this period, and qualitatively consistent with those of the 1950–2020 period, thus suggesting an acceleration.

The trends in low-latitude events described in section 3c might be affected by poleward displacements of the subtropical belt. Poleward trends in LAT_{MIN} would progressively embed low-latitude regions within the subtropical belt (eventually reducing subtropical ridges in equatorward regions) and expose higher latitudes to subtropical ridges. There are some hints of these expected effects in the SH (Fig. 11e). However, overall changes in LAT_{MIN} are arguably small as compared to the latitudinal extension of the considered events to explain the trends in events reported above. Changes in low-latitude events are much less obvious in the NH (Fig. 11b), despite the presence of some pronounced regional increases (e.g., over Eurasia in summer). Therefore, we conclude that subtropical widening trends are small to have measurable effects in events or confined to specific regions, where they can be confounded with regional phenomena and internal variability. This lack of compelling evidence is supported by the different rates of changes of events and subtropical belt: the overall faster subtropical widening of recent decades is not accompanied by comparably larger changes in events.

4. Surface impacts and case studies

Many authors have described specific impacts associated with blocking occurrence (e.g., Trigo et al. 2004; Sillmann et al. 2011; Sousa et al. 2016, 2017, 2018a; Brunner et al. 2017), and to a lesser extent with subtropical ridges over limited regions (e.g., Sousa et al. 2018a; 2019; Santos et al. 2009). Some of the reported effects may result from mixed influences of different types of high pressure systems (e.g., subtropical ridges and omega blocks). The impacts of omega and Rex blocks have not been explored separately in a systematic way, either. Therefore, the dissimilar frequencies and regions of occurrence of these blocking types (section 3a) could lead to a biased characterization of blocking impacts in previous works. In this section, we illustrate the wide range of impacts associated with high pressure systems through case studies of events selected from the catalog, as well as composite analyses for different types of daily 2D structures.

We first focus on the near-surface responses to different daily patterns over the Euro-Atlantic sector, a region reporting all types of structures during winter (as shown in Fig. 7). Winter composites (Figs. 13a–d) are formed from all daily 2D structures of the same type detected over western Europe in that season (10°W–5°E, and all latitudes higher than LAT_{MIN}). The structures display distinct flow patterns and jet configurations, in overall agreement with those described in the conceptual model (Fig. 1) of section 2b. Interestingly, Rex-hybrid blocks, not considered so far as a prototype of block, are the structures with the overall largest impacts in near-surface temperature over large areas of Europe, although they also comprise the lowest number of days in the composites (approximately two-thirds of pure Rex blocks; Fig. 13g). Their highly tilted structure (tied to the subtropical belt) simultaneously fosters strong poleward heat transport upstream and cold continental advection downstream. The complete cutoff of Rex-pure blocking high also promotes central European cooling, but the equatorward low pressure anomaly prevents cold air masses from reaching southern Europe (Fig. 13h), as reported in previous studies (e.g., Trigo et al. 2004; Masato et al. 2012; Sousa et al. 2018a). Differently, meridionally extended omega blocks shield central Europe from the cold advection, which tends to occur well upstream and downstream of the block (Fig. 13f). Interestingly, Greenland warming, a classical fingerprint of blocking action, is herein found to be restricted to pure Rex patterns (Fig. 13h), which represent less than half of all blocking types. Finally, we note that despite the relatively similar flow configurations of subtropical ridges and omega blocks, they cause different temperature anomalies (e.g., maximum warming in southern and central Europe, respectively; Figs. 13a,b) due to the imprinting role of the flow reversal in the latter. Regarding precipitation, winter ridges are associated with a tendency to drying over some areas of western Europe and central Mediterranean (Fig. 13i), as found in regional studies (e.g., Santos et al. 2009). Opposite signals are observed farther north, mainly over the eastern North Atlantic, in agreement with the strong jet induced in the upstream flank of the ridge. A somewhat reversed precipitation pattern has been reported for high-latitude blocks (e.g., Trigo et al. 2004; Masato et al. 2012; Sousa et al. 2017). However, the dissection of blocking types (Figs. 13j–l) unveils very different and even contrasting precipitation impacts. Contrary to Rex blocks, omega blocks inhibit rainfall on their southern flank, including most regions with above-normal precipitation under Rex configurations. Rex-hybrid blocks occurring in this longitudinal sector exhibit an intermediate pattern between those two, but notably they concentrate much of the drying signal over the United Kingdom typically attributed to all blocks.

A similar composite analysis is presented in Fig. S9 to illustrate the winter impacts of high pressure systems over South America. The results show similarities to those described for western Europe (Fig. 13), in particular for precipitation, with ridges and omega blocks inhibiting rainfall over low-latitude Mediterranean-like climatic areas, such as the coastal regions of Chile, and opposite but modest effects during Rex blocks. Different surface responses are also observed in other seasons (see, e.g., the summer composite of western Europe patterns in Fig. S10), confirming the major role of subtropical ridges and blocks in driving warm summer temperature anomalies over low and high latitudinal regions, respectively (e.g., Sousa et al. 2018a).

Next, we illustrate two examples of high-impact case studies in different regions and seasons. Figure 14 summarizes the main results for the European mega-heatwave of summer 2010 that hit western Russia (e.g., Barriopedro et al. 2011). From a climatological point of view, summer ridges and omega blocks over this region are responsible for the highest and

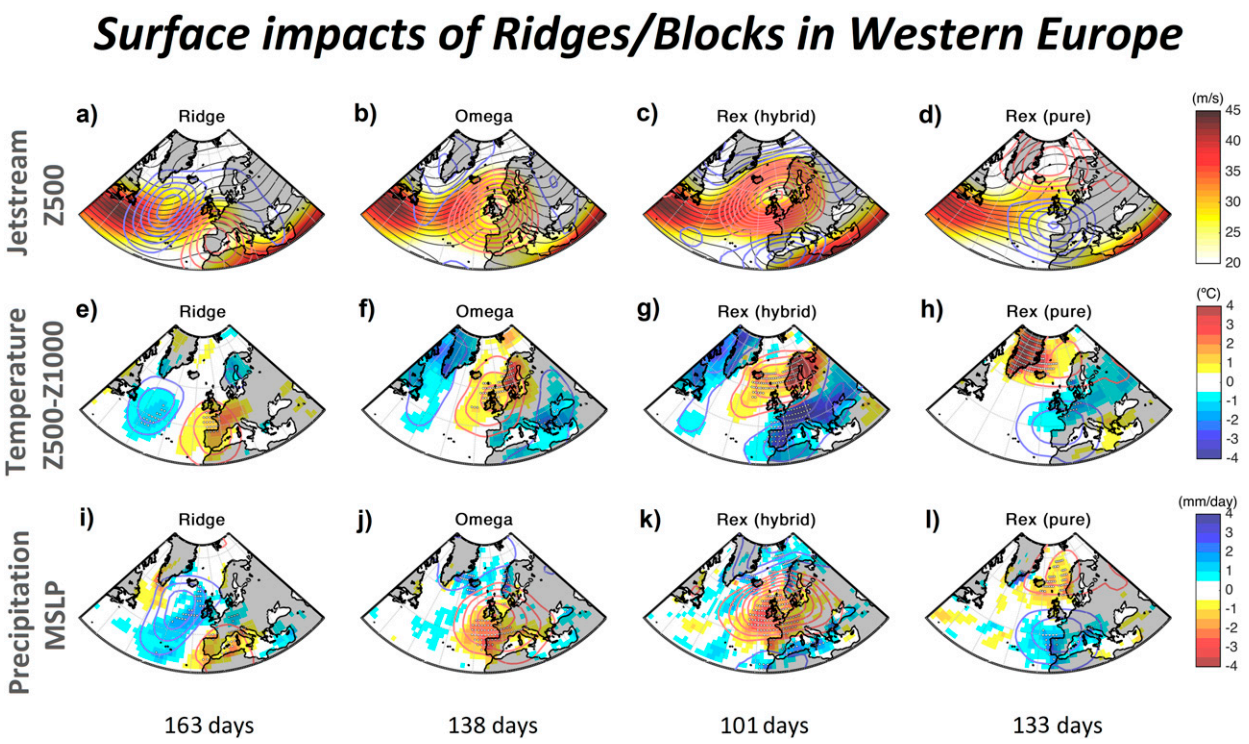

FIG. 13. Winter composites (1950–2020) over the Euro-Atlantic sector for different types of daily structures. Composites of zonal wind at 300 hPa (shading; m s^{-1}), Z500 (black contour lines, with 20-m intervals), Z500 anomaly (positive and negative anomalies in red and blue contour lines, respectively, with 20-m intervals) for daily structures over western Europe (10°W–5°E, and all latitudes higher than LAT_{MIN}) classed as (a) subtropical ridge, (b) omega block, (c) Rex-hybrid block, and (d) Rex-pure block. (e)–(h) As in (a)–(d), but for the composites of 2-m temperature anomalies (shading; °C) and 1000–500-hPa geopotential height thickness anomalies (positive and negative anomalies in red and blue contour lines, respectively, with 2-dam intervals). (i)–(l) As in (a)–(d), but for the composites of daily rainfall rate anomalies (shading; mm day^{-1}) and MSLP anomalies (positive and negative anomalies in red and blue contour lines, respectively, with 2-hPa intervals). Light white dots in (e)–(l) represent anomalies larger than one standard deviation from the seasonal mean climatology. Data source: NCEP–NCAR reanalysis.

most extended warm anomalies, this signal being weaker and mainly confined to Scandinavia during Rex structures (Figs. 14a–c). In particular, the typical signatures of omega blocks (Fig. 14b) match well the spatial pattern associated with the 2010 mega-heatwave. The method captures a pronounced increase (approximately threefold) in omega blocks during that summer, particularly over the 30°–60°E sector (Fig. 14d). This was accompanied by concurrent decreases in subtropical ridges and Rex blocks. A snapshot for 28 July 2010 (Fig. 14e) clearly illustrates the main omega features, including the pronounced poleward extension of subtropical air masses reaching 60°N and its subtropical connection. Recall that the method does not capture structures confined within the subtropical belt, which might also cause extreme events in regions equatorward of LAT_{MIN}. However, this does not prevent diagnosing the low-latitude impacts caused by meridional extensions of the subtropical belt beyond these regions (see e.g., the warm temperature anomalies over Iberia during summer subtropical ridges in western Europe; Fig. S10e).

As an additional example, Fig. 15 illustrates the synoptic setting during the devastating wildfire episode of California in late 2017 (CAL FIRE 2019). The analysis is restricted to the most prominent high pressure patterns in the region (subtropical ridges and omega blocks). Their composites show clear north–south dipoles in precipitation and temperature anomalies along the western coast of North America, although more intense and extending larger and poleward areas in the case of omega blocks (Figs. 15a–d). Low-level easterly flow conditions (so-called Santa Ana events) are known to foster wildfires in this region (Mass and Ovens 2019) by adiabatic warming downslope of mountain ranges. Despite the coarse resolution of the dataset, inferences from the mean sea level pressure (MSLP) composites also suggest a geostrophic easterly wind component at synoptic scales. The episode was associated with outstanding increases in the frequency of ridges and omega blocks over the region (Fig. 15e). The summed effects of the associated rainfall deficits and the enhanced advection of hot dry air masses agree with the observed fire fuel dryness (Nauslar et al. 2018). As the anomalous occurrence of subtropical ridges and omega blocks was comparable, with transitions between them, we conclude that the extreme event can be explained by their joint effects, which emphasizes the limitation of traditional approaches. The sustained subtropical inflow (through either ridges or omega blocks) was so large

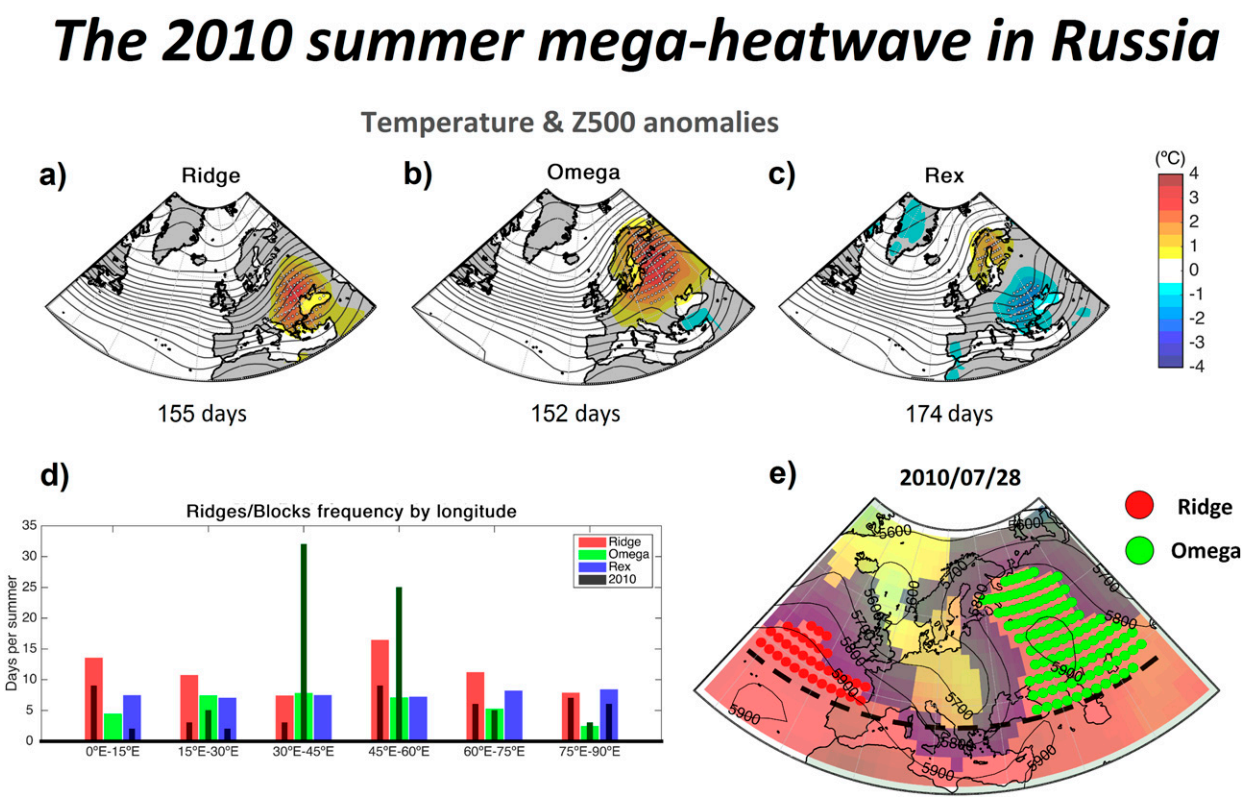

FIG. 14. European mega-heatwave of summer 2010. Composites of Z500 (black contour lines, with 25-m intervals) and 2-m temperature anomalies (shading; °C) for all summer days of 1950–2020 with (a) subtropical ridge, (b) omega block, and (c) Rex block patterns over eastern Europe (30°–60°E, and all latitudes higher than LAT_{MIN}). Light white dots represent temperature anomalies larger than one standard deviation from the seasonal mean climatology. (d) Climatological mean (colored wide bars) and 2010 (dark thin bars) summer frequencies (in days) of each type of pattern over longitudinal sectors of 15° width. (e) Snapshot detection of daily structures for 28 Jul 2010. Green and red circles identify omega block and subtropical ridge patterns, respectively. Grid points shaded with purple represent areas of strong wind (GHG > 20 m per degree). The dashed line denotes the minimum detection latitude (LAT_{MIN}). Data source: NCEP–NCAR reanalysis.

that it became imprinted as a marked poleward migration of the subtropical belt edge during December 2017 (Fig. 15f). Similar episodes of persistent subtropical ridges and omega patterns have also been associated with recent droughts in California (e.g., Seager et al. 2015; Swain et al. 2016).

5. Concluding remarks

In this work we have addressed recommendations of previous reviews and long-lasting requirements from the scientific community for a definition of ''blocking'' that recognizes and at the same time differentiates the diversity of patterns. For the first time, we propose an integrated approach for the life cycle of high pressure midtropospheric events that combines blocking (i.e., wave breaking) and subtropical ridges (i.e., poleward migrations of the subtropical belt) in a systematic way, therefore avoiding more restricted views of blocking. It is based on an empirical dynamically inspired conceptual model that accounts for stages and transitions between the different types of structures. The considered patterns include well-established types of blocks (omega and Rex) and at the same time more controversial but equally relevant high pressure structures at low (subtropical ridges) and high (polar blocks) latitudes. It also acknowledges the temporary mixture of subtropical air masses and extratropical flow reversals, resulting in an efficiently reduced number of idealized patterns, and corresponding transitions, whose combinations represent well the otherwise unmanageable diversity of events.

We acknowledge that an ideal definition should rely on the underlying dynamics governing the onset, development, and decay of these events. However, given its current limited understanding, a classification based on simpler metrics related to widely accepted and easily recognized morphological features seems the best approach, as it is easily implementable and facilitates intercomparisons. As such, we opted for a relatively straightforward and flexible algorithm (self-adaptive to background conditions) that can be applied to gridded fields of reanalysis/operational products, forecast systems, and climate model simulations. The derived product includes a catalog of classified events with their main characteristics (duration, type of event, etc.) complemented by a 3D array with the spatiotemporal evolution of the daily 2D classified structures that conform to the life cycle of events, satisfying the needs of a wide range of applications.

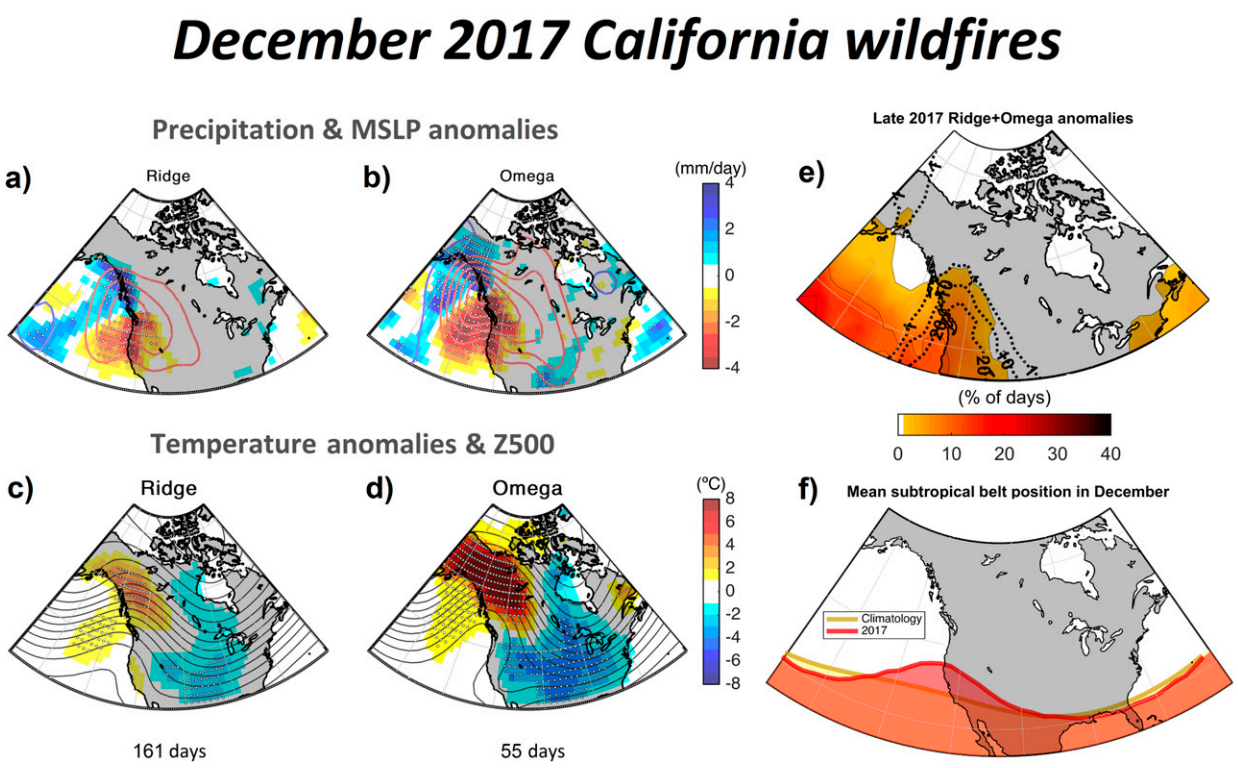

FIG. 15. The late 2017 California wildfire episode. (a),(b) Composites of MSLP anomalies (positive and negative anomalies in red and blue contour lines, respectively, with 2-hPa intervals) and daily rainfall rate anomalies (shading; mm day^{-1}) for all autumn [October–December (OND)] days of 1950–2020 with subtropical ridge [in (a)] and omega block [in (b)] patterns over the eastern Pacific (135°–120°W and all NH latitudes higher than LAT_{MIN}). Light white dots represent precipitation anomalies larger than one standard deviation from the seasonal mean climatology. (c),(d) As in (a) and (b), but for Z500 (black contour lines, with 20-m intervals) and 2-m temperature anomalies (shading; °C). (e) Relative anomaly (in percentage of seasonal days with respect to climatology) of the total frequency of subtropical ridges and omega blocks during OND 2017 (shading) and December 2017 (dotted black lines). (f) The so-called ''Ridiculously Resilient Ridge'' in California, showing the mean latitudinal extension of the subtropical belt for all December months of 1950–2020 (yellow line) and December 2017 (red shading). Data source: NCEP–NCAR reanalysis.

This allows us to provide a global assessment of these events, their preferred areas of occurrence and transitions, long-term frequency trends, and the distinctive impacts of each type of structure. In the NH, Rex blocks tend to occur in mid- to high-latitude areas between Greenland and Europe, and across northeastern Asia and Alaska, in agreement with previous blocking climatologies (e.g., Barriopedro et al. 2010 and references therein). The eastern oceanic basins (and continental extensions) of the NH are preferential areas for the occurrence of omega blocks, coinciding with the main regions of wave breaking (e.g., Davini et al. 2012; Masato et al. 2012). These omega-block regions appear as meridional extensions of the main areas of subtropical ridge activity. As supported by a systematic assessment of ''phase'' transitions, our results indicate that the life cycle of midlatitude blocking cannot be fully separated from the phenomenology of subtropical ridges, partly explaining the diversity of structures termed blocks. However, the dissection of the life cycle in differentiated patterns is of paramount importance for the attribution of associated impacts, which exhibit marked differences depending on the considered pattern. In the SH, midlatitude blocks are much less frequent than in the NH. Rex-like events are largely confined to Antarctica, although they are not associated with the midlatitude wave-breaking phenomenology of our conceptual model, but rather with flow reversals, likely reflecting persistent polar easterlies. Therefore, these so-called polar blocks should not be viewed as canonical blocks, and additional studies are encouraged to confirm whether they can be considered another family of blocking-like patterns.

We conclude that the reported frequency of midlatitude blocking in the SH might have been overestimated, these structures matching better with temporary phases of subtropical ridge events, exception made for the Pacific, where omega block stages can persist enough to form events. A similar conclusion applies to low-latitude blocks of the eastern basin of the North Atlantic (e.g., Davini et al. 2012), which well correspond herein to subtropical ridges transitioning to omega blocks. The lack of discrimination between omega and Rex blocks might also have been an additional confounding factor leading to a biased characterization of blocking frequencies (and impacts) toward Rex-like patterns in previous works for the NH.

Although the considered patterns often organize to form persistent events, their associated impacts are remarkably

different. Subtropical ridges and omega blocks are major drivers of the weather conditions in mid-to-low latitudes of western Europe and North America (up to one-third of the winter days), where they promote drying and warming all year-round (and their associated hazards, such as heatwaves or wildfires). On the contrary, higher-latitude Rex blocks are associated with cold and wet conditions over the same regions, in particular during winter (e.g., Sillmann et al. 2011; Sousa et al. 2017, 2018a, 2019). As a result, classical fingerprints of blocking such as the Greenland warming and the U.K. drying are mainly restricted to Rex block flows, and previous studies have therefore overseen the diversity of impacts associated with blocking-like patterns. Although blocks can also cause large impacts in the SH (Timbal and Drosdowsky 2013; Sousa et al. 2018b; Garreaud et al. 2019), the concentration of inhabited areas toward low latitudes where blocks are unusual points to a major role of subtropical ridges in modulating regional climates of the SH.

Our results also show contrasting results concerning long-term changes (1950–2020) in the frequency of these events, with relatively common increases of low-latitude events (mainly subtropical ridges) in some regions and seasons, and weak changes (mostly nonsignificant decreases) of blocking events, except in polar areas. Obviating changes in polar blocks, which are more sensitive to the reanalysis product and analyzed period, blocking trends are mainly in line with some recent studies indicating that blocking activity is not increasing under enhanced greenhouse gases concentrations (Matsueda et al. 2009, 2010; Dunn-Sigouin et al. 2013; Barnes et al. 2014; Woollings et al. 2018). For the more reliable period of satellite observations (1980–2020), our results do not support the theorized overall increase of blocking activity as a result of recent Arctic amplification (e.g., Francis and Vavrus 2012), which was also questioned by Barnes (2013). At the most, a small increase in Arctic blocks has been observed in the NH during recent decades (e.g., Greenland blocking in summer). Moreover, trends show considerable hemispheric differences. Changes are spatially more complex and seasonally varying in the NH, with relatively common weak and insignificant trends in the zonal averages, and regional changes that depend on the considered period. In the SH, hemisphere-wide trends emerge in association with recent trends in the SAM (Swart et al. 2015), mainly during austral summer, in turn attributed to increasing greenhouse gases concentrations and ozone depletion (Lim et al. 2016; Ndarana et al. 2012). There are also low-latitude trends in apparent association with the poleward expansion of the SH subtropical belt, particularly over the Pacific. The intensification and migration of subtropical climates poses hazards for many midlatitude regions, mainly those with Mediterranean-like climates (Seager et al. 2019; Sousa et al. 2018b; Polade et al. 2017), and simple metrics similar to the subtropical belt maximum latitude proposed here have proven useful to explore surface impacts and the behavior of subtropical anticyclones (Reboita et al. 2019). However, our results indicate that changes in subtropical ridges (or events in general) cannot be fully explained by a poleward expansion of the subtropical belt.

Our conceptual model sets the grounds for similar diagnostic exercises in impact studies and recent climate change topics of active research, including tropical/subtropical expansion rates (e.g., Staten et al. 2018), recent circulation responses to Arctic amplification (Coumou et al. 2018; Hassanzadeh and Kuang 2015), future changes in large-scale dynamics (e.g., Cattiaux et al. 2012; de Vries et al. 2013), or paleoclimatic studies (e.g., the suggested role of blocking during the Last Glacial Maximum; Ludwig et al. 2017). Such an approach could help to better constrain the relative roles of internal variability and externally forced responses in these high-impact regimes, including the uncertain projections of blocking-like patterns. Being as inclusive as possible, we hopefully expect that this study contributes to set the basis for a more unified terminology concerning the diversity of high-impact high pressure patterns, avoiding confusions in the scientific community, and facilitating the intercomparison of results.

Acknowledgments. P. M. Sousa and R. M. Trigo acknowledge financial support from FCT-UIDB/50019/2020–IDL. P. M. Sousa was supported through the following FCT project: HOLMODRIVE–North Atlantic Atmospheric Patterns Influence on Western Iberia Climate: From the Late Glacial to the Present (PTDC/CTA-GEO/29029/2017). D. Barriopedro and R. García-Herrera were supported by the Spanish government through the PALEOSTRAT (CGL2015-69699-R) and JEDiS (RTI2018-096402-BI00) projects. R. M. Trigo was supported by project INDECIS, which is part of ERA4CS, an ERA-NET initiated by JPI Climate, with co-funding by the European Union (Grant 690462). We are grateful to three anonymous reviewers, who made very constructive comments and helped improve the manuscript.

Data availability statement. All data and code used in this study are available upon request to the corresponding author.

REFERENCES

Antokhina, O., P. N. Antokhin, E. V. Devyatova, and M. Yulia, 2017: Wintertime atmospheric blocking events over western Siberia in the period 2004–2016 and their influence on the surface temperature anomalies. *Proceedings*, **1**, 198, https://doi.org/10.3390/ecas2017-04127.

Barnes, E. A., 2013: Revisiting the evidence linking Arctic amplification to extreme weather in midlatitudes. *Geophys. Res. Lett.*, **40**, 4728–4733, https://doi.org/10.1002/grl.50880.

——, J. Slingo, and T. Woollings, 2012: A methodology for the comparison of blocking climatologies across indices, models and climate scenarios. *Climate Dyn.*, **38**, 2467–2481, https://doi.org/10.1007/s00382-011-1243-6.

——, E. Dunn-Sigouin, G. Masato, and T. Woollings, 2014: Exploring recent trends in Northern Hemisphere blocking. *Geophys. Res. Lett.*, **41**, 638–644, https://doi.org/10.1002/2013GL058745.

Barriopedro, D., R. García-Herrera, A. R. Lupo, and E. Hernández, 2006: A climatology of Northern Hemisphere blocking. *J. Climate*, **19**, 1042–1063, https://doi.org/10.1175/JCLI3678.1.

——, ——, and R. M. Trigo, 2010: Application of blocking diagnosis methods to general circulation models. Part I: A novel detection scheme. *Climate Dyn.*, **35**, 1373–1391, https://doi.org/10.1007/s00382-010-0767-5.

——, E. M. Fischer, J. Luterbacher, R. M. Trigo, and R. García-Herrera, 2011: The hot summer of 2010: Redrawing the temperature record map of Europe. *Science*, **332**, 220–224, https://doi.org/10.1126/science.1201224.

Berrisford, P., B. J. Hoskins, and E. Tyrlis, 2007: Blocking and Rossby wave breaking on the dynamical tropopause in the Southern Hemisphere. *J. Atmos. Sci.*, **64**, 2881–2898, https://doi.org/10.1175/JAS3984.1.

Brunner, L., G. C. Hegerl, and A. K. Steiner, 2017: Connecting atmospheric blocking to European temperature extremes in spring. *J. Climate*, **30**, 585–593, https://doi.org/10.1175/JCLI-D-16-0518.1.

CAL FIRE, 2019: 2017 Wildfire activity statistics. California Department of Forestry and Fire Protection, https://www.fire.ca.gov/media/10059/2017_redbook_final.pdf.

Cattiaux, J., H. Douville, and Y. Peings, 2012: European temperatures in CMIP5: Origins of present-day biases and future uncertainties. *Climate Dyn.*, **41**, 2889–2907, https://doi.org/10.1007/s00382-013-1731-y.

Cheung, H. N., W. Zhou, Y. Shao, and W. Chen, 2013: Observational climatology and characteristics of wintertime atmospheric blocking over Ural–Siberia. *Climate Dyn.*, **41**, 63–79, https://doi.org/10.1007/s00382-012-1587-6.

Christensen, J. H., and Coauthors, 2013: Climate phenomena and their relevance for future regional climate change. *Climate Change 2013: The Physical Science Basis*, T. F. Stocker et al., Eds., Cambridge University Press, 1217–1308.

Copernicus Climate Change Service, 2017: ERA5: Fifth generation of ECMWF atmospheric reanalyses of the global climate. Copernicus Climate Change Service Climate Data Store (CDS), accessed March 2021, https://cds.climate.copernicus.eu/cdsapp#!/dataset/reanalysis-era5-pressure-levels?tab=form.

Coumou, D., G. D. Capua, S. Vavrus, L. Wand, and S. Wang, 2018: The influence of Arctic amplification on mid-latitude summer circulation. *Nat. Commun.*, **9**, 2959, https://doi.org/10.1038/s41467-018-05256-8.

Dai, A., D. Luo, M. Song, and J. Liu, 2019: Arctic amplification is caused by sea-ice loss under increasing CO_2. *Nature*, **10**, 121, https://doi.org/10.1038/s41467-018-07954-9.

Davini, P., and F. D'Andrea, 2020: From CMIP3 to CMIP6: Northern Hemisphere atmospheric blocking simulation in present and future climate. *J. Climate*, **33**, 10 021–10 038, https://doi.org/10.1175/JCLI-D-19-0862.1.

——, C. Cagnazzo, S. Gualdi, and A. Navarra, 2012: Bidimensional diagnostics, variability, and trends of Northern Hemisphere blocking. *J. Climate*, **25**, 6496–6509, https://doi.org/10.1175/JCLI-D-12-00032.1.

de Vries, H., T. Woollings, J. Anstey, R. J. Haarsma, and W. Hazeleger, 2013: Atmospheric blocking and its relation to jet changes in a future climate. *Climate Dyn.*, **41**, 2643–2654, https://doi.org/10.1007/s00382-013-1699-7.

Dole, R. M., and N. D. Gordon, 1983: Persistent anomalies of the extratropical Northern Hemisphere wintertime circulation: Geographical distribution and regional persistence characteristics. *Mon. Wea. Rev.*, **111**, 1567–1586, https://doi.org/10.1175/1520-0493(1983)111<1567:PAOTEN>2.0.CO;2.

Dong, L., T. Vogelsang, and S. J. Colucci, 2008: Interdecadal trend and ENSO-related interannual variability in Southern Hemisphere blocking. *J. Climate*, **21**, 3068–3077, https://doi.org/10.1175/2007JCLI1593.1.

Drouard, M., and T. Woollings, 2018: Contrasting mechanisms of summer blocking over western Eurasia. *Geophys. Res. Lett.*, **45**, 12 040–12 048, https://doi.org/10.1029/2018GL079894.

Dunn-Sigouin, E., S.-W. Son, and H. Lin, 2013: Evaluation of Northern Hemisphere blocking climatology in the global environment multiscale model. *Mon. Wea. Rev.*, **141**, 707–727, https://doi.org/10.1175/MWR-D-12-00134.1.

Egger, J., 1985: Slope winds and the axisymmetric circulation over Antarctica. *J. Atmos. Sci.*, **42**, 1859–1867, https://doi.org/10.1175/1520-0469(1985)042<1859:SWATAC>2.0.CO;2.

Francis, J. A., and S. J. Vavrus, 2012: Evidence linking Arctic amplification to extreme weather in mid-latitudes. *Geophys. Res. Lett.*, **39**, L06801, https://doi.org/10.1029/2012GL051000.

García-Herrera, R., R. Paredes, R. M. Trigo, I. F. Trigo, H. Hernández, D. Barriopedro, and M. T. Mendes, 2007: The outstanding 2004/05 drought in the Iberian peninsula: Associated atmospheric circulation. *J. Hydrometeor.*, **8**, 483–498, https://doi.org/10.1175/JHM578.1.

——, J. Díaz, R. M. Trigo, J. Luterbacher, and E. M. Fischer, 2010: A review of the European summer heat wave of 2003. *Crit. Rev. Environ. Sci. Technol.*, **40**, 267–306, https://doi.org/10.1080/10643380802238137.

Garreaud, R. D., J. P. Boisier, R. Rondanelli, A. Montecinos, H. H. Sepúlveda, and D. Veloso-Aguila, 2019: The Central Chile Mega Drought (2010–2018): A climate dynamics perspective. *Int. J. Climatol.*, **40**, 421–439, https://doi.org/10.1002/joc.6219.

Grise, K. M., and Coauthors, 2019: Recent tropical expansion: Natural variability or forced response? *J. Climate*, **32**, 1551–1571, https://doi.org/10.1175/JCLI-D-18-0444.1.

Hanna, E., T. E. Cropper, R. J. Hall, and J. Cappelen, 2016: Greenland Blocking Index 1851–2015: A regional climate change signal. *Int. J. Climatol.*, **36**, 4847–4861, https://doi.org/10.1002/joc.4673.

Hassanzadeh, P., and Z. Kuang, 2015: Blocking variability: Arctic amplification versus Arctic Oscillation. *Geophys. Res. Lett.*, **42**, 8586–8595, https://doi.org/10.1002/2015GL065923.

Kalnay, E., and Coauthors, 1996: The NCEP/NCAR 40-Year Reanalysis Project. *Bull. Amer. Meteor. Soc.*, **77**, 437–471, https://doi.org/10.1175/1520-0477(1996)077<0437:TNYRP>2.0.CO;2.

Li, W. H., L. F. Li, M. F. Ting, and Y. M. Liu, 2012: Intensification of Northern Hemisphere subtropical highs in a warming climate. *Nat. Geosci.*, **5**, 830–834, https://doi.org/10.1038/ngeo1590.

Lim, E.-P., H. H. Hendon, J. M. Arblaster, F. Delage, H. Nguyen, S.-K. Min, and M. C. Wheeler, 2016: The impact of the southern annular mode on future changes in Southern Hemisphere rainfall. *Geophys. Res. Lett.*, **43**, 7160–7167, https://doi.org/10.1002/2016GL069453.

Liu, P., and Coauthors, 2018: Climatology of tracked persistent maxima of 500-hPa geopotential height. *Climate Dyn.*, **51**, 701–717, https://doi.org/10.1007/s00382-017-3950-0.

Ludwig, P., J. G. Pinto, C. C. Raible, and Y. Shao, 2017: Impacts of surface boundary conditions on regional climate model simulations of European climate during the last glacial maximum. *Geophys. Res. Lett.*, **44**, 5086–5095, https://doi.org/10.1002/2017GL073622.

Marshall, A. G., D. Hudson, M. C. Wheeler, O. Alves, H. H. Hendon, M. J. Pook, J. S. Risbey, 2014: Intra-seasonal drivers of extreme heat over Australia in observations and POAMA-2. *Climate Dyn.*, **43**, 1915–1937, https://doi.org/10.1007/s00382-013-2016-1.

Masato, G., B. J. Hoskins, and T. J. Woollings, 2012: Wave-breaking characteristics of mid-latitude blocking. *Quart. J. Roy. Meteor. Soc.*, **138**, 1285–1296, https://doi.org/10.1002/qj.990.

Mass, C. F., and D. Ovens, 2019: The Northern California wildfires of 8–9 October 2017: The role of a major downslope wind event. *Bull. Amer. Meteor. Soc.*, **100**, 235–256, https://doi.org/10.1175/BAMS-D-18-0037.1.

Matsueda, M., R. Mizuta, and S. Kusunoki, 2009: Future change in wintertime atmospheric blocking simulated using a 20-km-mesh atmospheric global circulation model. *J. Geophys. Res.*, **114**, D12114, https://doi.org/10.1029/2009JD011919.

——, H. Endo, and R. Mizuta, 2010: Future change in Southern Hemisphere summertime and wintertime atmospheric blockings simulated using a 20-km-mesh AGCM. *Geophys. Res. Lett.*, **37**, L02803, https://doi.org/10.1029/2009GL041758.

Mendes, M. C. D., R. M. Trigo, I. F. A. Cavalcanti, and C. C. DaCamara, 2008: Blocking episodes in the Southern Hemisphere: Impact on the climate of adjacent continental areas. *Pure Appl. Geophys.*, **165**, 1941–1962, https://doi.org/10.1007/s00024-008-0409-4.

Nakamura, N., and C. S. Y. Huang, 2018: Atmospheric blocking as a traffic jam in the jet stream. *Science*, **361**, 42–47, https://doi.org/10.1126/science.aat0721.

Nauslar, N. J., J. T. Abatzoglou, and P. T. Marsh, 2018: The 2017 North Bay and Southern California fires: A case study. *Fire*, **1**, 18, https://doi.org/10.3390/fire1010018.

Ndarana, T., and D. W. Waugh, 2011: A climatology of Rossby wave breaking on the Southern Hemisphere tropopause. *J. Atmos. Sci.*, **68**, 798–811, https://doi.org/10.1175/2010JAS3460.1.

——, ——, L. M. Polvani, G. J. P. Correa, and E. P. Gerber, 2012: Antarctic ozone depletion and trends in tropopause Rossby wave breaking. *Atmos. Sci. Lett.*, **13**, 164–168, https://doi.org/10.1002/asl.384.

Patterson, M., T. Woollings, T. Bracegirdle, and N. T. Lewis, 2020: Wintertime Southern Hemisphere jet streams shaped by interaction of transient eddies with Antarctic orography. *J. Climate*, **33**, 10 505–10 522, https://doi.org/10.1175/JCLI-D-20-0153.1.

Peings, Y., J. Cattiaux, S. J. Vavrus, and G. Magnusdottir, 2018: Projected squeezing of the wintertime North-Atlantic jet. *Environ. Res. Lett.*, **13**, 074016, https://doi.org/10.1088/1748-9326/aacc79.

Pelly, J. L., and B. J. Hoskins, 2003: A new perspective on blocking. *J. Atmos. Sci.*, **70**, 743–755, https://doi.org/10.1175/1520-0469(2003)060<0743:ANPOB>2.0.CO;2.

Peters, D., and D. W. Waugh, 2003: Rossby wave breaking in the Southern Hemisphere wintertime upper troposphere. *Mon. Wea. Rev.*, **131**, 2623–2634, https://doi.org/10.1175/1520-0493(2003)131<2623:RWBITS>2.0.CO;2.

Pinheiro, M. C., P. A. Ullrich, and R. Grotjahn, 2019: Atmospheric blocking and intercomparison of objective detection methods: Flow field characteristics. *Climate Dyn.*, **53**, 4189–4216, https://doi.org/10.1007/s00382-019-04782-5.

Polade, S. D., A. Gershunov, D. R. Cayan, M. D. Dettinger, and D. W. Pierce, 2017: Climate variability and change of Mediterranean-type climates. *Sci. Rep.*, **7**, 10 783, https://doi.org/10.1038/s41598-017-11285-y.

Reboita, M. S., T. Ambrizzi, B. A. Silva, R. F. Pinheiro, and R. P. da Rocha, 2019: The South Atlantic subtropical anticyclone: Present and future climate. *Front. Earth Sci.*, **26**, 8, https://doi.org/10.3389/feart.2019.00008.

Santos, J. A., J. G. Pinto, and U. Ulbrich, 2009: On the development of strong ridge episodes over the eastern North Atlantic. *Geophys. Res. Lett.*, **36**, L17804, https://doi.org/10.1029/2009GL039086.

Schwierz, C., M. Croci-Maspoli, and H. C. Davies, 2004: Perspicacious indicators of atmospheric blocking. *Geophys. Res. Lett.*, **31**, L06125, https://doi.org/10.1029/2003GL019341.

Seager, R., M. Hoerling, S. Schubert, H. Wang, B. Lyon, A. Kumar, J. Nakamura, and N. Henderson, 2015: Causes of the 2011–14 California drought. *J. Climate*, **28**, 6997–7024, https://doi.org/10.1175/JCLI-D-14-00860.1.

——, T. J. Osborn, Y. Kushnir, I. R. Simpson, J. Nakamura, and H. Liu, 2019: Climate variability and change of Mediterranean-type climates. *J. Climate*, **32**, 2887–2915, https://doi.org/10.1175/JCLI-D-18-0472.1.

Sillmann, J., M. Croci-Maspoli, M. Kallache, and R. W. Katz, 2011: Extreme cold winter temperatures in Europe under the influence of North Atlantic atmospheric blocking. *J. Climate*, **24**, 5899–5913, https://doi.org/10.1175/2011JCLI4075.1.

Sousa, P. M., D. Barriopedro, R. M. Trigo, A. M. Ramos, R. Nieto, L. Gimeno, K. F. Turkman, and M. L. R. Liberato, 2016: Impact of Euro-Atlantic blocking patterns in Iberia precipitation using a novel high resolution dataset. *Climate Dyn.*, **46**, 2573–2591, https://doi.org/10.1007/s00382-015-2718-7.

——, R. M. Trigo, D. Barriopedro, P. M. M. Soares, A. M. Ramos, and M. L. R. Liberato, 2017: Responses of European precipitation distributions and regimes to different blocking locations. *Climate Dyn.*, **48**, 1141–1160, https://doi.org/10.1007/s00382-016-3132-5.

——, ——, ——, ——, and J. A. Santos, 2018a: European temperature responses to blocking and ridge regional patterns. *Climate Dyn.*, **50**, 457–477, https://doi.org/10.1007/s00382-017-3620-2.

——, R. C. Blamey, C. J. C. Reason, A. M. Ramos, and R. M. Trigo, 2018b: The 'Day Zero' Cape Town drought and the poleward migration of moisture corridors. *Environ. Res. Lett.*, **13**, L124025, https://doi.org/10.1088/1748-9326/aaebc7.

——, D. Barriopedro, A. M. Ramos, R. García-Herrera, F. Espírito-Santo, and R. M. Trigo, 2019: Saharan air intrusions as a relevant mechanism for Iberian heatwaves: The record breaking events of August 2018 and June 2019. *Wea. Climate Extremes*, **26**, 100224, https://doi.org/10.1016/j.wace.2019.100224.

Staten, P. W., J. Lu, K. M. Grise, S. M. Davis, and T. Birner, 2018: Reexamining tropical expansion. *Nat. Climate Change*, **8**, 768–775, https://doi.org/10.1038/s41558-018-0246-2.

Stuecker, M. F., and Coauthors, 2018: Polar amplification dominated by local forcing and feedbacks. *Nat. Climate Change*, **8**, 1076–1081, https://doi.org/10.1038/s41558-018-0339-y.

Swain, D. L., D. E. Horton, D. Singh, and N. S. Diffenbaugh, 2016: Trends in atmospheric patterns conducive to seasonal precipitation and temperature extremes in California. *Sci. Adv.*, **2**, e1501344, https://doi.org/10.1126/sciadv.1501344.

Swart, N. C., J. C. Fyfe, N. Gillett, and G. J. Marshall, 2015: Comparing trends in the southern annular mode and surface westerly jet. *J. Climate*, **28**, 8840–8859, https://doi.org/10.1175/JCLI-D-15-0334.1.

Takaya, K., and H. Nakamura, 2005: Geographical dependence of upper-level blocking formation associated with intraseasonal amplification of the Siberian high. *J. Atmos. Sci.*, **62**, 4423–4440, https://doi.org/10.1175/JAS3629.1.

Teng, H., and G. Branstator, 2017: Causes of extreme ridges that induce California droughts. *J. Climate*, **30**, 1477–1492, https://doi.org/10.1175/JCLI-D-16-0524.1.

Tibaldi, S., and F. Molteni, 1990: On the operational predictability of blocking. *Tellus*, **42A**, 343–365, https://doi.org/10.3402/tellusa.v42i3.11882.

Timbal, B., and W. Drosdowsky, 2013: The relationship between the decline of southeastern Australian rainfall and the strengthening of the subtropical ridge. *Int. J. Climatol.*, **33**, 1021–1034, https://doi.org/10.1002/joc.3492.

Trigo, R. M., I. F. Trigo, C. C. DaCamara, and T. J. Osborn, 2004: Winter blocking episodes in the European-Atlantic sector:

Climate impacts and associated physical mechanisms in the reanalysis. *Climate Dyn.*, **23**, 17–28, https://doi.org/10.1007/s00382-004-0410-4.

Tyrlis, E., J. Bader, E. Manzini, and D. Matei, 2021: Reconciling different methods of high-latitude blocking detection. *Quart. J. Roy. Meteor. Soc.*, **147**, 1070–1096, https://doi.org/10.1002/qj.3960.

Wang, L., W. Chen, W. Zhou, J. C. L. Chan, D. Barriopedro, and R. Huang, 2010: Effect of the climate shift around mid 1970s on the relationship between wintertime Ural blocking circulation and East Asian climate. *Int. J. Climatol.*, **30**, 153–158.

Woollings, T., J. G. Pinto, and J. A. Santos, 2011: Dynamical evolution of North Atlantic ridges and poleward jet stream displacements. *J. Atmos. Sci.*, **68**, 954–963, https://doi.org/10.1175/2011JAS3661.1.

——, D. Barriopedro, J. Methven, S. W. Son, O. Martius, J. Sillmann, A. R. Lupo, and S. Seneviratne, 2018: Blocking and its response to climate change. *Curr. Climate Change Rep.*, **4**, 287–300, https://doi.org/10.1007/s40641-018-0108-z.